Journal of Alloys and Compounds 984 (2024) 173989

Contents lists available at ScienceDirect

Journal of Alloys and Compounds

journal homepage: www.elsevier.com/locate/jalcom

Role of microstructure in the exploitation of self-healing potential in form-stable composite phase change materials based on immiscible alloys

Matteo Molteni [a,*], Antonio Mattia Grande [b], Paola Bassani [c], Elisabetta Gariboldi [a]

[a] Politecnico di Milano, Department of Mechanical Engineering, Via La Masa 1, Milan 20156, Italy
[b] Politecnico di Milano, Department of Aerospace Science and Technology, Via La Masa 34, Milan 20156, Italy
[c] National Research Council of Italy, Institute of Condensed Matter Chemistry and Technologies for Energy CNR-ICMATE, Via Previati 1/E, Lecco 23900, Italy

ARTICLE INFO

Keywords:
Multi-functional materials
Phase change material composites
Self-healing materials
Extrinsic self-healing
Immiscible Al-Sn alloys

ABSTRACT

Metallic Phase Change Materials (PCMs), based on solid-liquid transitions, represents one of the most promising technologies for efficient Thermal Energy Storage (TES), due to their superior thermal conductivity and energy storability per unit volume, but suffer of limited solutions for their handling at the molten state. The use of Miscibility Gap Alloys (MGAs) allows to manage PCM volume expansion and keep it confined when molten, preventing interaction with the environment. A relevant example is provided by the Al-Sn system, where Al covers the role of the high-temperature stable and highly thermal-conductive passive matrix and Sn the active PCM. The alloy can thus be considered a Composite PCM (C-PCM). The response fastness of these systems depends on their thermal diffusivity, subjected to abrupt variations under the presence of discontinuities and damages. In this sense, the authors investigated the possibility to employ molten Sn mobility in a potentially damaged C-PCM for self-healing purposes, aimed to restore, at least partially, the material continuity and thus its thermal diffusivity. Exudation heat treatments above the melting temperature of Sn were performed on sets of Al-40%wt. Sn metallic composites, produced either with powder metallurgy or liquid metal routes, in order to quantify and assess the mobility of the Sn under simulated operating conditions. Exudation tests assess Simple Mixed powders and liquid metal routes sample as the ones with the highest healing potential. Al dissolution and re-deposition was established by EDS analyses as one of the principal Sn mobility mechanisms. Laser Flash Analysis tests, as well as microstructural investigations, were performed on the samples before and after both healing-focused and simulated service heat treatments to evaluate the changes of thermal diffusivity. Healing-focused treatment at 250°C for 1 hour generally displayed a moderate thermal diffusivity recovery and simulated service by shorter cycles between 170°C and 270°C slightly reduce it. The beneficial role of healing focused heat treatments at 250°C for 1 hour suggests that the presence of fully molten Sn phase during service for relatively long time could be beneficial for functional healing. The requirements of suitable Al-Sn microstructures for self-healing purposes, granting at the same time the C-PCM functionalities, i.e., thermal energy storage and form-stability, were set.

1. Introduction

Phase change materials (PCMs) represent one of the most promising responses to the incoming energy crisis, promoting effective Thermal Energy Storage (TES), due to their capability to store and release heat under proper thermal stimuli by undergoing phase changes in both heating and cooling. The majority of the systems proposed in the literature rely on solid-liquid transitions, since they offer the best compromise in terms of energy storable as latent heat and limited volume changes of the system during the phase transition [1,2]. Accordingly to their chemical compositions, PCMs can be classified in organic and inorganic [3,4]. Metallic phase change materials belong to the latter group. The definition of metallic PCMs embraces different types of metals or alloys. In general, the melting behavior of the specific metallic system defines its suitability as a PCM. Incongruently melting metals and alloys can undergo segregation, due to the compositional differences of the system when it undergoes solid-liquid transition that leads to performance degradation [5]. For this reason, congruently melting metals,

* Corresponding author.
E-mail addresses: matteo1.molteni@polimi.it (M. Molteni), antoniomattia.grande@polimi.it (A.M. Grande), paola.bassani@cnr.it (P. Bassani), elisabetta.gariboldi@polimi.it (E. Gariboldi).

https://doi.org/10.1016/j.jallcom.2024.173989
Received 11 October 2023; Received in revised form 8 February 2024; Accepted 24 February 2024
Available online 26 February 2024

whose composition is the same both in the solid and the liquid state, are selected for PCM purposes. Similarly, also eutectics are employed, since they solidify in two inseparable phases. More recently, Miscibility Gap Alloys (MGAs), on which the current study is focused, are considered as PCMs [6]. The use of metals in thermal energy management systems offers higher heat storage capability per unit volume than organic PCMs, in combination with higher operating temperatures [5,7–13]. Moreover, the superior thermal conductivity and diffusivity of metallic PCMs promotes faster heat transfer, leading to rapid melting/solidification events and, correspondingly, high power absorption/release.

However, handling liquid metal is not a trivial task, representing the most critical drawback in their practical application. The presence of a liquid phase at temperatures above the transition one, requires confinement strategies which should also consider the volume expansion and shrinkage during the melting and solidification of the PCM, respectively. Further, the metal liquid phase reactions with external agents may result in compositional changes which are detrimental for thermal conductivity [14]. Thus, encapsulation techniques (from macro to nano scale [15,16]) and containers [17,18] based on both metals [17, 18] or ceramics [15] are widely adopted as effective solutions for the confinement of liquid metallic PCMs.

As mentioned before, in the last decade Sugo et al. [19] proposed a different approach to the problem. Indeed, they suggested the use of binary immiscible alloys, whose elements practically do not interact between each other both in the solid and, at least in a certain temperature range, when the low-melting phase is in its liquid range. For these materials they also proposed a target microstructure where inclusions of the low-melting phase (active PCM phase) were embedded in a passive matrix of the high-melting phase, able to contain the potential leakage of the former. Such a phase arrangement promotes the achievement of form-stability, i.e., the capability of the C-PCM of maintaining its shape after thermal cycles. This microstructure, resulting in well distinguishable phases, can equate one of conventional composite materials. For this reason, immiscible alloys-based PCMs can be classified as Composite Phase Change Materials (C-PCMs). Further, such a microstructure is also similar to those suggested for thermally triggered extrinsic self-healing materials, i.e., an external stimulus is needed for the healing action [20]. In these materials, an external healing agent in the liquid state (potentially insulated from the matrix by a third phase), is present as distributed inclusions. When intercepted by discontinuities, that may arise during service, the healing agent gives the possibility to restore, under proper conditions, the material continuity [21]. If a discontinuity arose in the abovementioned C-PCM, the material continuity could be potentially restored, as the low-melting active PCM phase inclusions behave as healing agents, triggered by a local temperature increase. Indeed, when active phase becomes liquid, it expands, and flows through the discontinuity, and solidify therein, connecting previously detached surfaces.

The exploitation of the extrinsic self-healing mechanism in a metallic C-PCM material is not to be intended in terms of structural but rather of functional properties. The reliability of the properties of metallic PCMS is mined by the presence of discontinuities that can arise during service. Indeed, these latter can sensibly reduce thermal conductivity, thus impairing heat transfer potential and altering service conditions. The partial or complete filling by low-melting metal phase of discontinuities can thus partly recovers of thermal conductivity, i.e. leading to functional healing [22,23]. The available scientific literature is mainly focused on self-healing in the view of structural properties rather than transport properties. In this sense, to the authors' best knowledge, thermal conductivity recovery is only limited to polymer-based composites whose self-healing performances have been demonstrated [24–31]. The effect of metallic healing agents for electrical conductivity recovery in damaged electronic circuits was presented in literature [32, 33]. However, the recovery of thermal transport properties of alloys or fully metallic composites at present has not been investigated. This recovery is of particular importance when the material is used ad PCM, whose thermal response will depend on the stability of thermal properties, within others, thermal diffusivity and thermal conductivity.

A relevant example of MGAs is the Al-Sn system [34] (Fig. 1, computed with Thermocalc software [35], which relies on a CALPHAD-based approach [36]). Activation temperature lays close to 230°C, coinciding with pure Sn melting temperature. The compositions of phases formed in Al-Sn alloys are further relatively stable nearly above the Sn melting point, limiting possible segregations effects arising in the cyclic conditions that characterize service conditions of PCMs. The literature reports different processes for an efficient dispersion of Sn, the active PCM/healable agent, in the passive high temperature stable Al matrix [37–42]. Powder metallurgy route is suggested as a possible solution [43,44]. The imposition of high cooling rates, in the order of hundreds of °C/s, demonstrates to be effective as well [45–48].

Moreover, multicomponent alloys based on a ternary Al-Cu-Si-Sn-Bi immiscible alloy have also been already proposed in literature to be used as self-healing materials [23]. These alloys are characterized by liquid phase separation which leads to two liquid solidifying at different temperatures. At the completion of the solidification, the low-melting liquid, rich in Sn and Bi, remains in the form of isolated droplets. The self-healing potential of the alloy is exploited by these almost spherical inclusions and is triggered by the local temperature increase above the melting temperature of the Sn-Bi eutectic structure (completely liquid at 250°C) and by the consequent volume expansion and increased flowability [23].

Thus, the presence of isolated inclusions of a low-melting phase, possibly of stable chemical composition in solid and liquid phase, in immiscible alloys can be exploited for the development of multifunctional composites with both PCMs and self-healing purposes. The flowability of the (molten) low-melting phase should be carefully controlled to achieve the desired target. In terms of self-healing potential, the capability of the active phase of filling discontinuities in the bulk of the composite is beneficial, but, on the other hand, the liquid should not uncontrollably leak on the external surface of the material. Indeed, the leakage of the active phase reduces at the same time the heat storage potential and thermal conductivity of C-PCMs due to the reduction of the content of the melting/solidifying PCM phase and the void formation. The use of Computerized Tomography (CT) during a thermal cycle of Al-Sn C-PCMs has recently demonstrated that the leakage of Sn-phase from their surface is strictly related to the

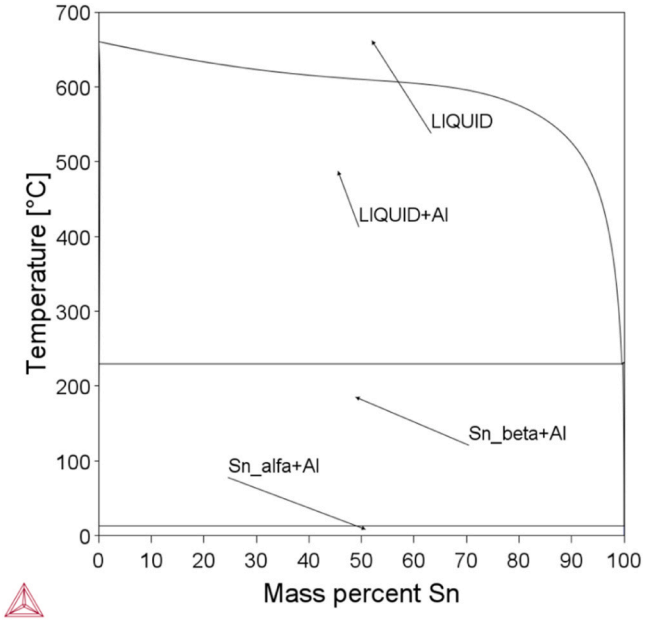

Fig. 1. Al-Sn phase diagram, computed with Thermocalc software.

microstructural features [49]. Similarly, the same experimental technique had been used to characterize in-situ extrinsic healing behavior of organic materials. In this case, the healing action is induced by the flow of material released by encapsulated inclusions [50]. CT was also adopted for testing metallic alloys intrinsic self-healing at smaller scale, related to diffusion and precipitate formation mechanisms [51].

Ex-situ techniques can be performed for determining materials self-healing potential in metals as well. Among these, observations of metallographic sections before and after thermal cycles allow the monitoring of how discontinuities are filled by healing agent under thermal input [23,52,53]. In particular, Kim et al. [23] proposed the evaluation on polished surfaces of the exudation of the self-healing agent, stimulated by local plastic strains and stresses induced by indentations.

Inspired by the aforementioned studies, where low-melting phases are exploited in their liquid state as healing agents for filling cracks, and by previous results demonstrating the possibility to limit the leakage of active low-melting phases in Al-Sn C-PCM through microstructure control, the authors set up tests to investigate the potential introduction of extrinsic self-healing functionality in the C-PCMs. The study was specifically intended to evaluate the Sn capability to easily exudate and flow on the free-surfaces of C-PCMs [54,55], to reach discontinuities and fill them. The influence of the microstructure, strongly dependent on the production technology adopted, was considered as well. A set of heat treatments was applied to quantify the effects of temperature, time, and microstructure on Sn mobility on free surfaces. Metallographic observations, properly analyzed, were proposed as ex-situ tests, from which indexes related to Sn-mobility were derived for the estimation of self-healing potential. The actual functional self-healing was then confirmed by thermal diffusivity measurements on C-PCMs before and after selected heat treatments with self-healing target.

2. Materials and methods

The experimental tests have been performed on a set of 6 alloys produced by different techniques (Table 1) with nominal composition Al-40% mass Sn, approximately corresponding to 20% Sn volume content. The composition was selected on the bases of preliminary studies, performed on Al-Sn and addressed toward PCM performances characterization [19,56,57]. In particular, the selected C-PCM should grant the highest performances in terms of energy storage, proportional to the amount of the active low-melting phase, i.e., Sn, and, at the same time, avoid the leakage of Sn when it is molten. In other words, the amount of this latter does not have to exceed the percolation threshold, i.e., Sn regions do not have to interconnect and form a continuous network. For Al-Sn system, the percolation threshold is reached when Sn amount approximately reaches the 30% in volume, 54% in wt. [19,56,57]. Details of their processing are reported elsewhere [43,46,48,58–60], and are shortly summarized in Table 1. All the proposed systems have been already characterized in terms of PCM response. In this view, DSC cyclic tests, widely adopted in literature for the evaluation of the PCM performances, are proposed for the MRS sample (Fig. 2) as representative example. The curve displays two peaks, one in heating and the other one in cooling, related to Sn melting and solidification respectively. For further details on the DSC features of the proposed systems, the reader can refer to literature work [43,46,48,58–60].

Table 1
Summary of the processing conditions adopted to produce the investigated Al-40%Sn alloys.

Sample name			Ref.
SM+CC+HT500 *	Powder metallurgy route	Mixed Al and Sn powders, compressed at RT and finally heat treated at 500°C	[58]
BM+HC220 *		Ball milled powders compressed at 220°C	[43]
BM+CC *		Ball milled powders compressed at room temperature	[59]
BM+SM+CC+HT250 *		Mixture of Al powders with Sn+Al ball milled powder, cold compacted and heat treated at 250°C	[60]
PBLF (Powder Bed Laser Fusion)	Liquid metal route	Powder Bed Laser Fusion of mixed Al and Sn powders	[46]
MRS (Medium Rapid Solidification)		Cast parts with solidification rate of some hundreds of °C/s	[48]

*SM: simple mixture, BM: ball milling, CC: cold compression, HTXXX: heat treatment at XXX °C.

The acronyms related to the powder metallurgy route samples refer to the production technique adopted: BM and SM stand for Ball Milling and Simple Mixing, respectively; CC and HC220 are related to Cold Compression (room temperature) and Hot Compression at 220°C; whereas HT250/500 reports a heat treatment performed at 250°C or 500°C. The alloys produced via powder metallurgy route (here referred as BM+CC, BM+HC220, SM+CC+HT500, BM+SM+CC+HT250, each one in form of cylindrical billets) and liquid metal route (Powder Bed Laser Fusion samples, referred as PBLF, produced in form of cubes, and Medium Rapid Solidification granules, named MRS) were cut along a plane parallel to their compaction or building or solidification direction, respectively, as shown in Fig. 3. The final samples, in the form of parallelepipeds for the powder metallurgy routes and PBLF, and disks as far as MRS are concerned, are then obtained from the center of the starting products. In the view of self-healing characterization, three different types of heat treatments were considered, each one above Sn melting temperature: exudation heat treatments, addressed toward the Sn mobility quantification, healing-focused heat treatments, related to the functionality recovery and simulated service heat treatments to testify the system stability. 7 sets of samples were produced for all the material conditions, to be adopted for the following analyses: (i) Microstructural and DSC analyses of as produced condition, (ii) exudation heat treatment tests and surface analyses (subset of 5 sample), with following quantitative analyses, (iii) thermal diffusivity measurements in as produced and healed-focused condition and microstructural analyses in this latter condition. For the selected conditions, a further set of samples has been lastly produced for diffusivity measurements in as produced condition and after a first healing-focused heat treatment, 10 simulated service treatments and a further healing treatment.

Metallographic observations in as produced conditions, i.e., first set of samples, were performed after conventional polishing operations. As far as the DSC is concerned, MRS sample of approximately 55 mg mass was tested with DSC25, TA instruments, from Room Temperature to 300°C and viceversa with a heating rate of 10 °C/min for ten times.

The second set of samples was then addressed to exudation heat

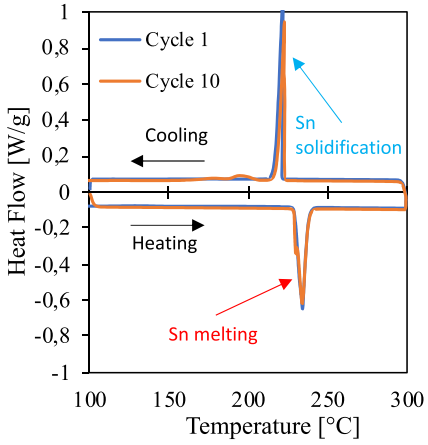

Fig. 2. DSC curve representative of the PCM performance of the MRS sample.

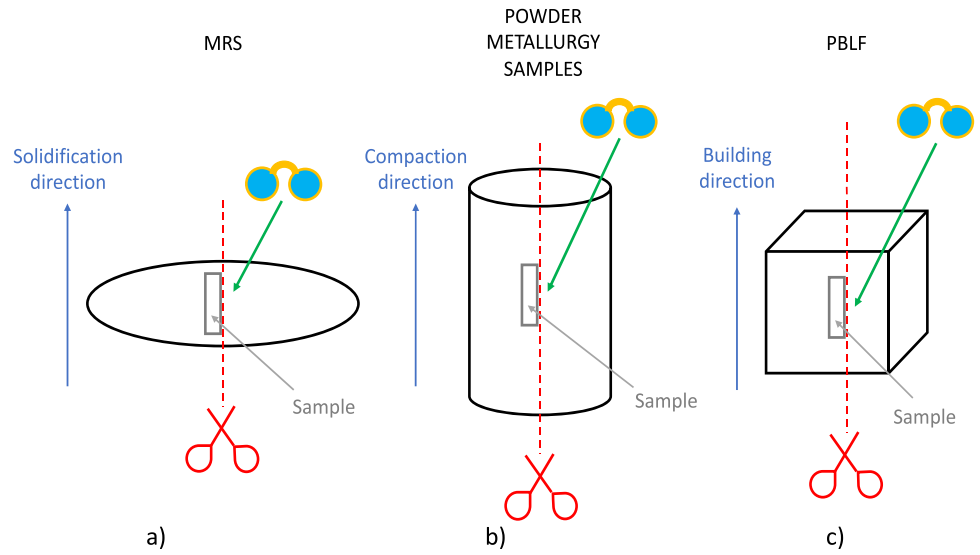

Fig. 3. Description of the sampling process for the Al-Sn specimens: a) granules obtained from Medium Rapid Solidification process, b) cylindrical billets obtained from powder metallurgy route and c) Powder Bed Laser Fusion parallelepipeds.

treatments for both Sn mobility on free surfaces monitoring (after surface polishing up to 1 μm diamond paste in order to limit the effect of the surface roughness).

Five different exudation heat treatments were performed on each material, considering a reference heat treatment (250°C X 60 min) and exploring separately the effect of time and temperature by performing cycles at additional times (30 and 180 min) or temperatures (240 and 270°C), respectively. All the investigated temperature exceeded the melting temperature of pure tin (232°C). One sample per type is considered for the heat treatments. These exudation heat treatments can be considered as simulated self-healing treatment, as they were performed at temperatures within or just above the maximum C-PCM service temperatures for close or slightly longer times. The heat input stimulates the leakage of the molten Sn phase addressed toward the assessment of its mobility in the studied system, whose quantification with image analysis allows the determination of the self-healing potential (Section 3.4.). For each testing condition, the set of variously produced sample was placed in a tubular furnace (Terside Carbolite Furnace), fluxed with Ar at 3 bar, and then quickly cooled, in an Ar atmosphere, by placing them in contact with an Al plate at room temperature. Treatments were performed in inert gas to avoid oxidation phenomena, in the attempt to reproduce the situation experienced by the surfaces of inner discontinuities in the material.

Microstructural investigation on as received and heat-treated samples was carried out combining low magnification Optical Microscopy (OM) analyses with high magnification Scanning Electron Microscopy (SEM). The first one was performed to highlight the general structure and the presence of discontinuities on the surface of the sample parallel to the cut direction (Fig. 3). A Leitz Aristomet Optical Microscope (equipped with polarizing/analyzing filters (Leica), and a DS- Fi3digital camera (Nikon), operating by Elements (Nikon) software was used in bright light, which revealed the Sn and Al phases of the unetched samples as the brighter yellowish and the slightly darker gray areas, respectively, while discontinuities (cracks, pores) appeared as black (Figs. 4 and 6).

SEM analyses were performed using a SEM (Zeiss Evo 50) equipped with Secondary Electrons (SE) and Back-Scattered Electrons (BSE) detectors. Analyses were specifically addressed to Sn morphology evaluation, specifically for the exuded Sn, which laid as separate particles on the surface, often with a droplet-shape. Conversely to the OM micrographs, Sn reveals as the brighter phase in the micrographs, being the element with the highest Z-number, whereas the darker regions identify as the Al. The discontinuities remain in black (Figs. 4–7). In order to help the readability of the micrographs, the microstructural features are highlighted with different colors: Al phase is identified with orange arrows/circles, whereas the yellow and the red ones are adopted for Sn and the discontinuities, respectively.

As previously mentioned, on each heat-treated sample, 5 representative areas of each sample were selected after the surface inspection in various region of sample surfaces parallel with respect to the cut direction, in order to quantify the exuded Sn to establish the self-healing potentiality of the different technologies for Al-Sn system. The magnification was selected in the range 100–300X, according to sample type, to obtain proper micrographs for quantitative analyses of the exudated Sn particles and droplets.

The geometrical features of Sn phase particles were quantified by means of the open-source software ImageJ [61], considering them as 2-D regions in SEM micrographs. Specifically, the equivalent diameter of particles, area fraction was directly derived by the software. The volume of exudated material per unit area was then calculated considering each Sn particle as a sphere of equivalent diameter.

EDS analyses were also performed on the Sn-rich exudated phase and on the Sn phase on surfaces of selected samples to gather information on possible compositional changes induced by heat treatments in order to assess Sn mobility mechanism inside the alloy for the most representative Al-Sn systems. For comparison purposes, the expected composition of the exuded Sn phase, expressed in mass percentages, in equilibrium condition at the heat treatment temperatures were computed with Thermo-Calc software [62] (Version 2020b with TCAL5.1 Al-Alloys Database). The Thermo-Calc software was used also to get other thermochemical data such as the theoretical density, as well as Al-Sn phase diagram (Fig. 1).

The recovery of heat transfer properties has been considered for the last set of samples by first comparing thermal diffusivity of as-produced samples to that of healing-focused heat treatment, selected as 250°C for 1 hour, performed in the same conditions of the exuded heat treatment. LFA analyses were performed for the achievement of the task. Due to the different samples size, various specimen geometries were adopted, maintaining the same one for the as produced and heat-treated material. Parallelepipeds of 10 ×10 mm basis with 3 mm thickness for powder metallurgy samples, cubes of 3 mm edge for PBLF and disks of 6 mm diameter and roughly 2 mm thickness for MRS samples. The surface to be hit by laser beam and the opposite one were ground and polished up to 3 μm diamond paste, then a thin layer of graphite was sprayed on

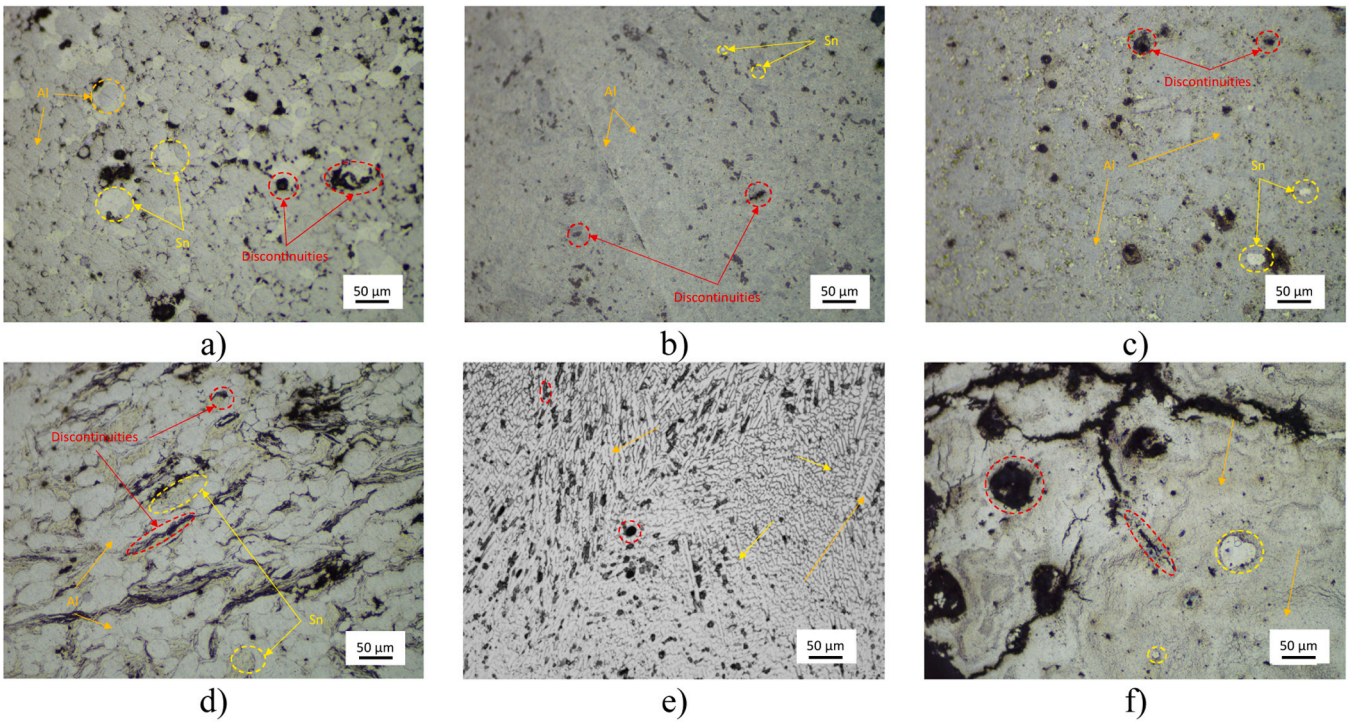

Fig. 4. Representative optical microscope micrographs at 200x magnification of the Al-40%wt.Sn samples in as-produced conditions: a) SM+CC+HT500, b) BM+CC, c) BM+HC220, d) BM+SM+CC+HT250, e) MRS and f) PBLF. In the figure Sn, whose features are highlighted in yellow, is the brighter yellowish phase, Al (orange) the darker greyish one and black areas are discontinuities (red), which can include Sn particles detached during polishing operations.

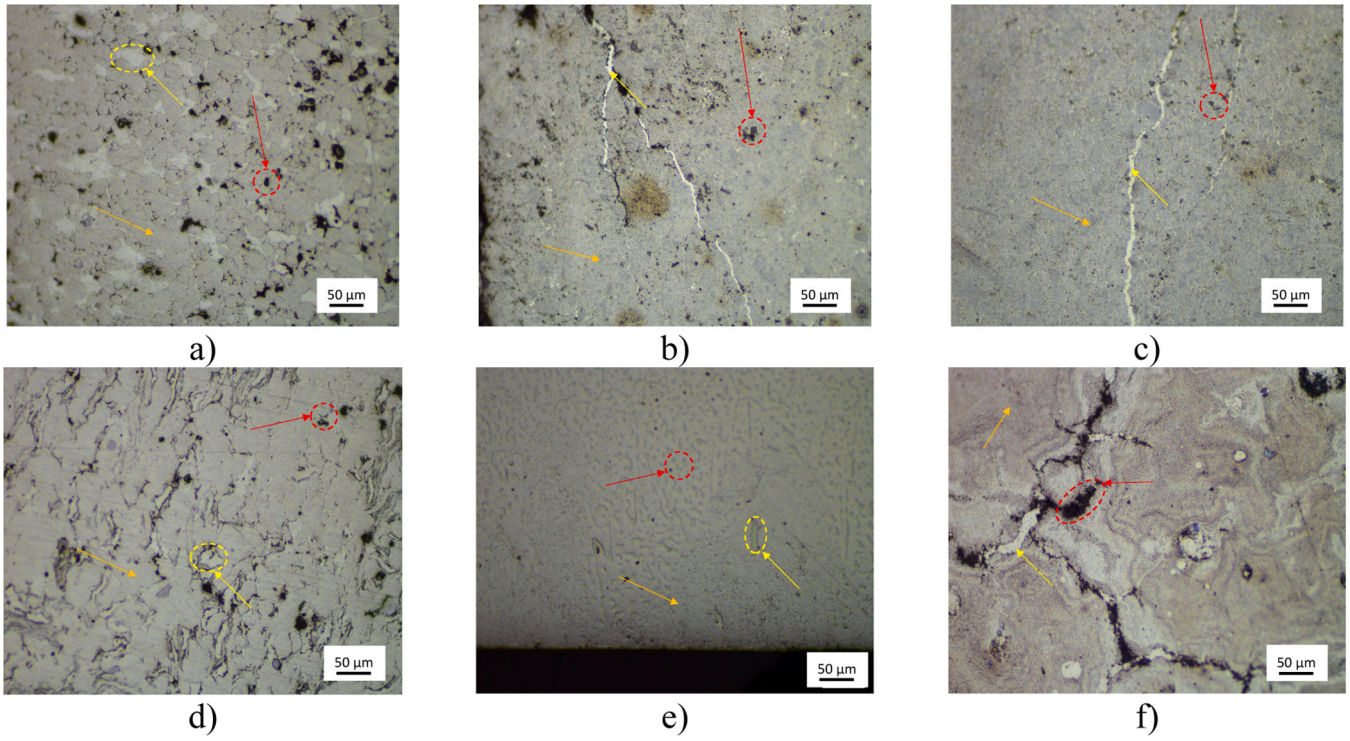

Fig. 5. Optical microscope micrographs of the Al-40%massSn samples, 60 min at 250°C heat treated: a) SM+CC+HT500, b) BM+CC, c) BM+HC220, d) BM+SM+CC+HT250, e) MRS and f) PBLF.

them. The samples were placed in suitable holders of the Linseis LFA 1000 equipment used for LFA Analyses. Tests were performed at 20°C, by adopting a trapezoidal pulse of 1 ms of duration at the operating voltage with a Nd:YAG laser of 350 V (AlphaLaser). The thermal diffusivity was directly calculated for the sample of known thickness by the machine on the basis of the time at which the back surface of the sample reaches one half the maximum temperature detected by an IR detector [63].

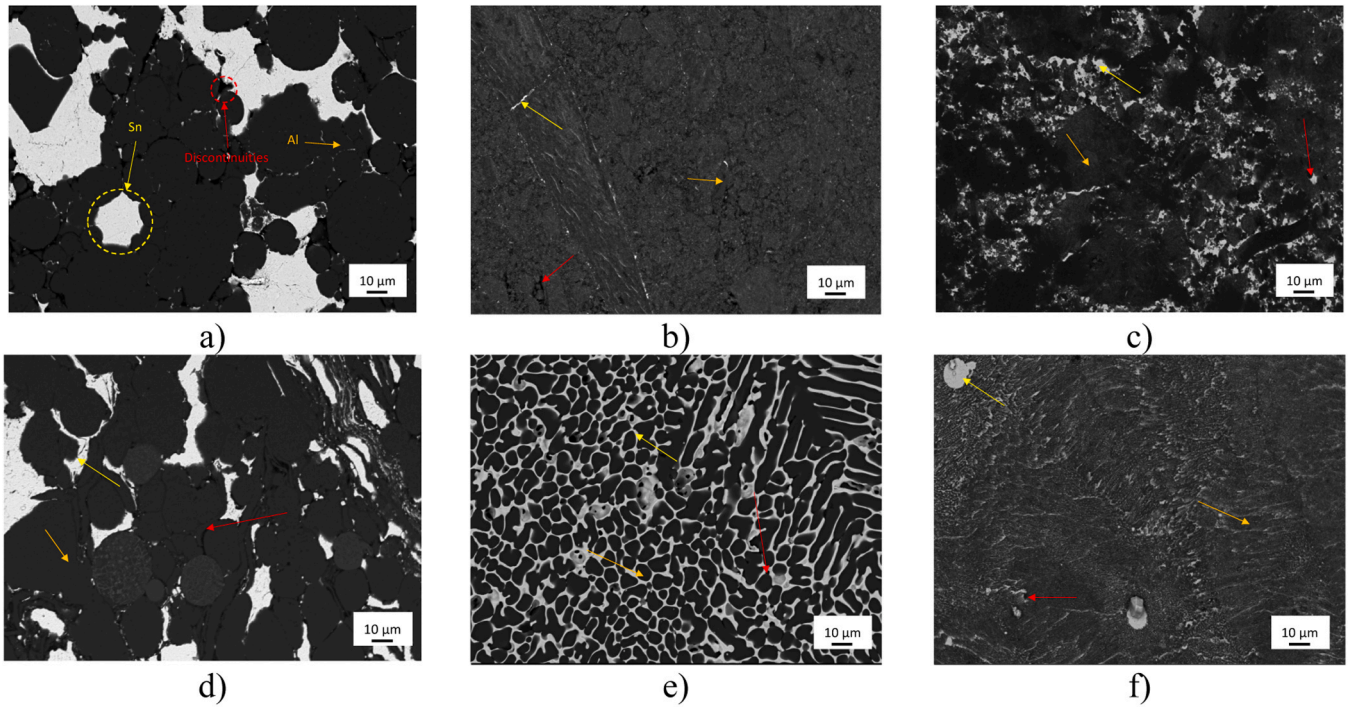

Fig. 6. Representative microstructure of the investigated Al-40%massSn samples: a) SM+CC+HT500, b) BM+CC, c) BM+HC220, d) BM+SM+CC+HT250, e) MRS and f) PBLF. Al (orange) has dark gray appearance, bright regions are referred to Sn (yellow) and black ones are discontinuities/voids (red).

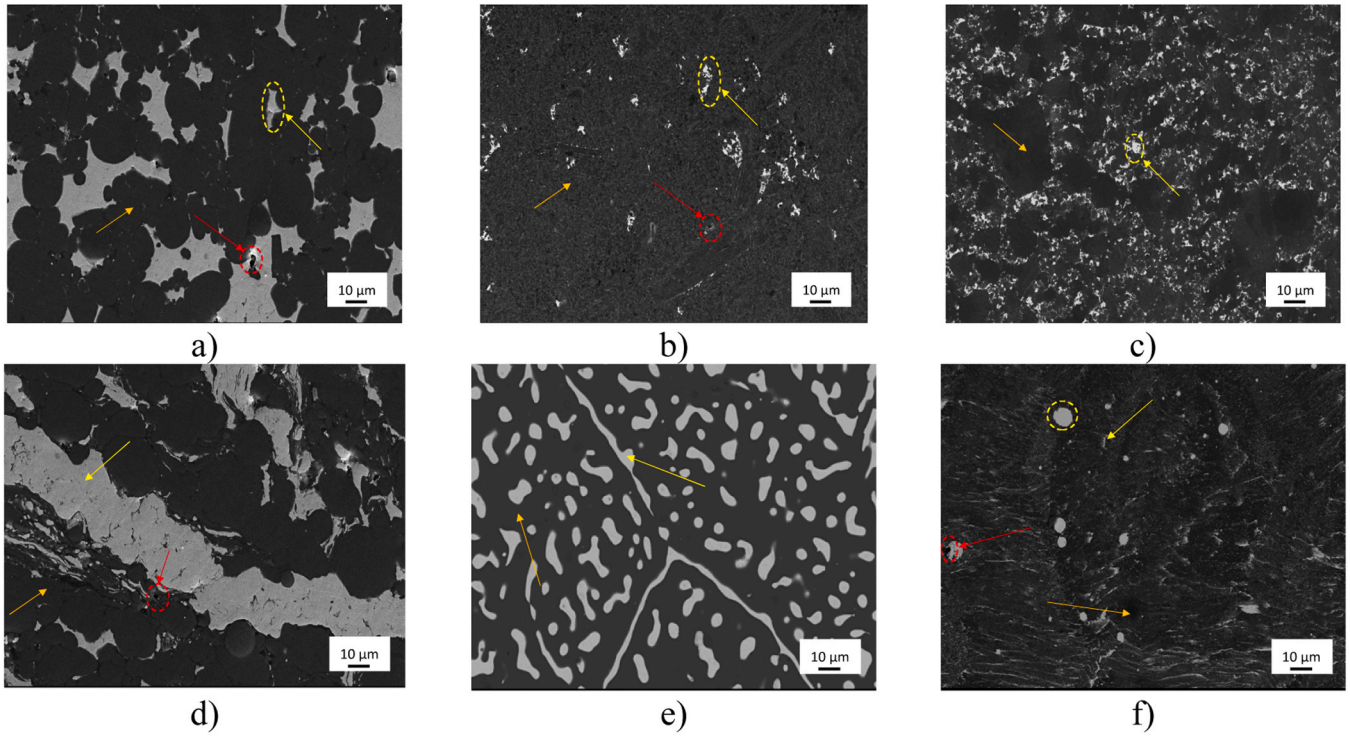

Fig. 7. Representative microstructure of the heat treated at 250°C for 60 minutes for Al-40%massSn samples: a) SM+CC+HT500, b) BM+CC, c) BM+HC220, d) BM+SM+CC+HT250, e) MRS and f) PBLF.

The stability of thermal transport properties of the healed samples was assessed further thermally cycling the most representative ones (BM+CC, MRS, PBLF and SM+CC+HT500) 10 times between 170 and 270°C in argon at 3 bar at heating/cooling rates of 20 °C/min, simulated service heat treatments. After thermal diffusivity measurements (described later), another healing-focused treatment cycle (samples, referred as H+10 S+H) was performed. When 2 or 3 samples per material and condition are available, the thermal diffusivity data were jointly analyzed.

The experimental density of samples was measured with Archimedes' principle (Analytical Balance ME204 with Density Kit Standard and Advanced, Mettler Toledo) repeating the measurement three times

before and after heat treatments. Care was paid to avoid removal of exudated Sn droplets and particles exudated to the surface of samples. The porosity (ρ_{calc}) of the Al-Sn samples was derived on the bases of the experimental density (ρ_{exp}) and the theoretical one (ρ_{th}), computed with Thermocalc and equal for all samples (Eq. (1)) [64]:

$$p_{calc} \quad [\%] = \left(1 - \frac{\rho_{exp}}{\rho_{th}}\right) * 100 \tag{1}$$

3. Results and discussion

3.1. As-produced samples microstructural observations

The microstructural features of the as-produced samples are strongly dependent on the specific process followed, as expected. In order to better highlight the qualitative differences in the microstructure, the different features are pointed out with different colors: Al phase is identified with orange, whereas yellow and red are selected for Sn areas and discontinuities, respectively.

All the proposed microstructures are already discussed in terms of PCM purposes [43,44,46,48,58,60], dispersing the active phase, i.e., Sn, in the high-melting temperature matrix, i.e., Al, which favors the containment of the former. Sn dispersion in C-PCMs resembles the introduction of encapsulated healing agents [65], making Al-Sn systems promising also in the view of self-healing purposes. At the same time, the C-PCM microstructure have to ensure the possibility for molten Sn to migrate inside the system in order to provide the satisfying healing action.

Starting from the powder metallurgy samples, the SM+CC+H500C one, produced simply mixing the coarser and softer tin powders to the Al ones, by compacting them at room temperature, and lastly by sintering the material (500°C), is made by slightly flattened and generally isolated brighter yellowish Sn regions dispersed in the darker greyish Al matrix, extending for a tenth of μm. They are clearly visible in Figs. 4a and 6a. Much finer structures are those of the samples obtained by concurrent ball milling of Al and Sn powders, followed by their compaction either at room temperature or at 220°C: BM+CC (Figs. 4b and 6b) and BM+HC220 (Figs. 4c and 6c) samples, respectively. In the latter case, the compression induced on the material just below the melting temperature of Sn has reasonably favored diffusional squeezing of tin outside ball milled powders, favoring its agglomeration. Indeed, hot compression step allows Sn regions to approximately reach an extension of some micrometers, whereas the two phases are practically indistinguishable in the BM+CC sample at the optical microscopy level (Fig. 4b). The more complex processing underwent by BM+SM+CC+HT250 sample (see Table 1) resulted in a much more inhomogeneous structure (Figs. 4d and 6d), characterized by the extremely fine microstructure of ball milled Al-Sn powders, by Al matrix made of the powders simply mixed to ball milled powders before compression and finally by small regions characterized by higher-Sn concentration, possibly accumulated due to the heat treatment action.

As far as the samples produced by liquid metal route are concerned, the as-produced MRS samples (Figs. 4e and 6e) displays the alternation of thick columnar Al dendrites and narrow Sn interdendritic channels. Several small pores are observed in the long columnar Al-interdendritic regions (wide solidification range of the Al-Sn system [34], often within Sn phase (Fig. 6e)). Their amount and size tend to increase (and they potentially become interconnected) in the last solidified portions of the material. The microstructure is more equiaxial at the center of the cast part. On the other hand, the Powder Bed Laser Fusion (PBLF) samples show mostly a very fine microstructure with the disappearance of the Al dendrites due to the high cooling rate experienced during the manufacturing process (Figs. 4f and 6f). At a macroscopical level, being the production process not-optimized yet [47], the material is characterized by the presence of some cracks and porosities, mainly related to the wide solidification temperature range of the Al-Sn binary system [34].

Microstructural analyses in as-produced conditions highlight the potential of the proposed systems in terms of self-healing functionality. Indeed, BM samples, as well as the PBLF one, exhibit dispersed smaller Sn basins, in addition to refined microstructural features. On the other hand, SM+CC+HT500, BM+SM+CC+HT250 offer extended and clearly visible Sn areas, possibly offering faster Sn movement with respect to BM samples when the material is damaged. MRS offers columnar interdendritic regions which may serve as a preferential path for the Sn movement inside the system, possibly leading to consistent leakage phenomena.

3.2. Healed-focused heat-treated samples microstructural observations

After the healing heat treatments performed with the various parameters mentioned the 'materials and methods' chapter, the bulk microstructures of all the tested samples qualitatively remain unchanged, apart from MRS one, where the Sn phase, identified with yellow, tends to become globular (Figs. 5 and 7). The flowing capability of molten Sn is clearly visible in Fig. 5b, c and f mainly at low magnification. Indeed, Sn demonstrates to locally fill cracks of different thicknesses arisen in the composite during its production process (Fig. 5b, c and f), promoting metallic continuity. In particular, ball milled, not sintered samples (BM+CC) seem to be more easily subjected to crack propagation due to their more brittle mechanical behavior, either during the sample preparation or the heat treatment, both as a consequence of stress development and release. However, the limited extension of the Sn basins in the BM+CC and PBLF, is not enough to fill the cracks that arose in the samples (Fig. 5b and f). Conversely, Sn in BM+HC220 successfully fill the cracks, possibly due to the action of the hot compression which promoted a more homogeneous spreading of the active phase in the as produced microstructure, as shown in Fig. 5c. The remaining powder metallurgy samples, on the other hand, do not experience any changes from the as-produced condition. MRS sample shows the strongest microstructural re-arrangement, exhibiting a transition from the dendritic microstructure toward a sphere-like Sn-dispersion with an accumulation of this latter (Figs. 5e and 7e), testifying the capability of the system in favouring Sn movement. The accelerated diffusion process and the wettability of Al by the low-melting Sn-rich phase could be responsible of the microstructural changes. Possibly, the microstructural rearrangement is the result of a combination between liquid metal corrosion and Rayleigh's instability. Indeed, first, the liquid Sn action, which is known to dissolve and re-deposit Al triggering liquid metal corrosion in Al [66–69], possibly promote Al grain boundaries sliding. Then, Sn Rayleigh's instability phenomena [70–72] also favor the modification in the shape of Sn-rich domains, shifting from thin interdendritic columns to globular-like appearance. This hypothesis needs further deepening which is out of the aim of the paper.

As expected, Sn spheres, marked with yellow circles, appeared on the free surface of the samples of the heat treated conditions of all processes, leaked either from the most superficial zones of the samples [73], and in the case of favorable paths, also from the composite inner regions. The spherical shape of the exuded Sn suggests the presence of superficial oxide on Al-Sn samples, preventing the spreading of Sn on Al [54,55]. Its presence can be related to the high affinity between oxygen and Al also at room temperature under standard pressure. The size and the number of the Sn droplet exuded form the composite system produced by powder metallurgy processes reflects the size of Sn-rich phase in the as produced microstructure, where Sn-rich regions are not highly interconnected (as will be seen in Section 3.4). As can be seen from Figs. 8 and 9, SM+CC+HT500 sample exhibits big droplets resembling deflated spheres, with diameters in the order of some tenths of micrometers. Deflection can be easily related to Sn volumetric change upon solidification, which approximately coincides with 20% shrinkage during the phase change [74,75], more evident for bigger droplets. The micrographs, taken at the same magnification, show that the droplets are

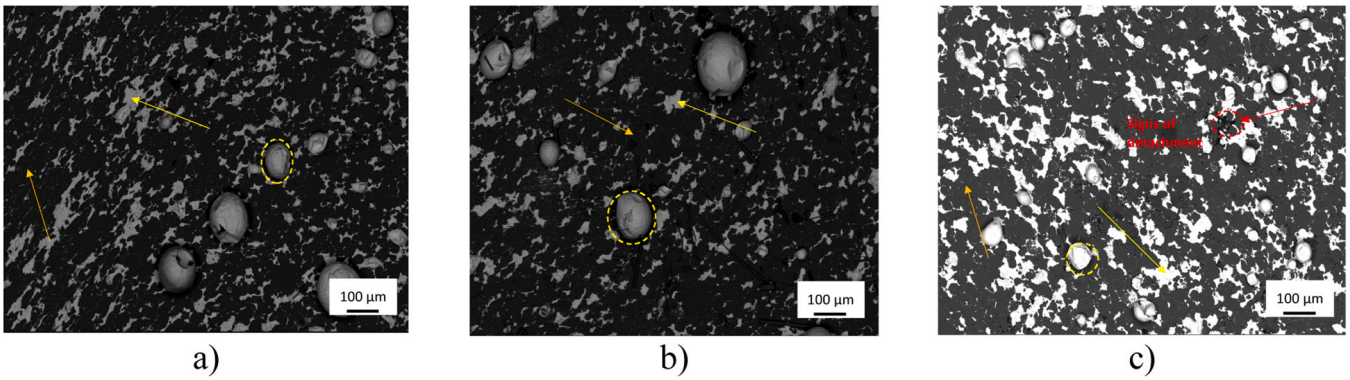

Fig. 8. Surface of the SM+CC+HT500 samples exposure in Ar atmosphere at: 250°C for 30 minutes (a), 60 minutes (b) and 180 minutes (c).

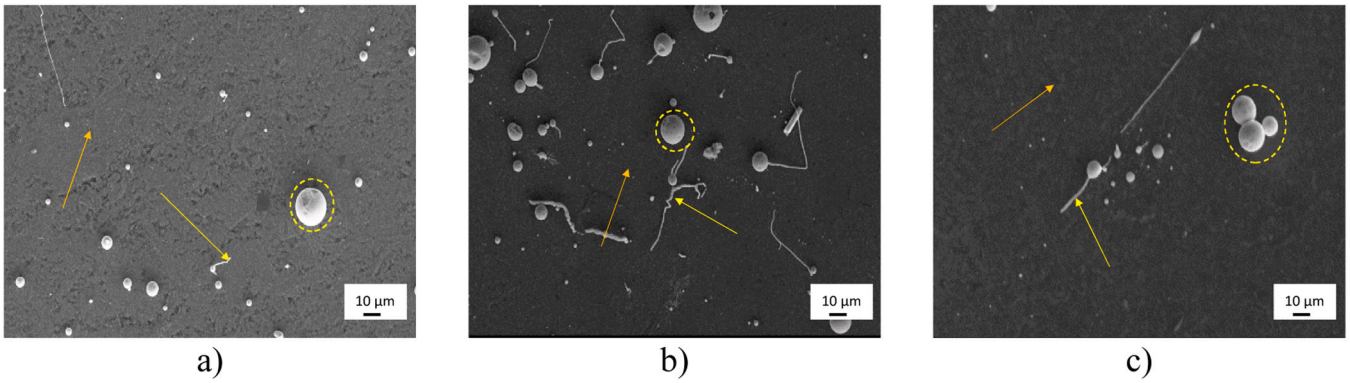

Fig. 9. Surface of the BM+CC samples after 60 minutes exposure in Ar atmosphere at: 240°C (a), 250°C (b) and 270°C (c).

widespread on all the sample surface. Further, they are slightly more numerous close to the Sn-rich areas (Fig. 8), whose interfacial energy offers favorable bonding for effective bonding with Sn. On the other hand, BM+CC shows a very limited leakage with smaller droplets, whose diameters very rarely exceed 10μ m (Fig. 9). The depressions on the surface of exuded spheres can be related to the shrinkage experienced by the tin droplets during its solidification and cooling to room temperature.

3.3. Density and porosity estimation

Both the powder metallurgy processes and those involving the solidification of the Al-40%Sn alloy from the molten state inevitably led to the presence of porosity (and in some cases, crack-like discontinuities) in the material, related to the technology itself. The porosity of a PCM material should be quantified and carefully considered. Indeed, this latter leads to a double side effect. On one hand, its presence strongly affects the resulting thermal conductivity and diffusivity of the composite [76,77]. On the other one, pores and discontinuities can settle part of the low-melting phases during its expansion as the melting occurs during the first heat cycle involving its phase transition and latent heat storage/release, without inducing excessive stresses in the phases.

Furthermore, especially if interconnected, porosity can represent a preferential path for the migration of the active liquid phase across the whole composite, either in the bulk or on the external surface. Similar effects are brought about by crack-like discontinuities. In this sense, liquid Sn, which acts as both PCM and healing agent when its melting temperature is exceeded, can fill the adjacent void regions locally promoting bridging and, consequently, more efficient heat transfer across the composite. In this view, the porosity (p_{calc}) of the different proposed Al-Sn systems is evaluated both for as produced samples and for those healing-focused heat treated at 250°C for 60 minutes and compared.

The values of the calculated porosity are listed for all samples in Table 2. Healing-focused heat treatment at 250°C for 60 minutes leads to a density reduction (and porosity increase) in the majority of the examined samples, related to the more or less copious Sn leakage.

Table 2
Porosity values, obtained from the comparison among experimental and theoretical densities, in both as-produced and healing focused heat treated conditions, for all the different studied techniques.

Production method	Experimental density (ρ_{ex}) [g/cm^3]		Theoretical density (ρ_{th}) [g/cm^3]	Porosity (p_{calc}) [%]
SM+CC+HT500	As-produced	3.243 ± 0.048	3.611	10.182
	Healing treated	3.199 ± 0.031		11.400
BM+HC220	As-produced	3.064 ± 0.006		14.594
	Healing treated	2.968 ± 0.008		17.806
BM+CC	As-produced	2.743 ± 0.111		24.028
	Healing treated	2.684 ± 0.006		25.672
BM+SM+CC+HT250	As-produced	3.060 ± 0.009		15.295
	Healing treated	3.065 ± 0.013		15.120
MRS	As-produced	3.454 ± 0.008		3.348
	Healing treated	3.512 ± 0.070		2.742
PBLF	As-produced	3.217 ± 0.075		10.902
	Healing treated	2.781 ± 0.114		22.967

Results concerning powder metallurgy route samples, SM+CC+HT500 offers the highest density value in both as produced and healing-focused heat-treated conditions. Further, among the samples produced by powder metallurgy route, the initially denser samples including SM in the production step plus a following sintering at 500 and 250°C, i.e., with holding temperature leading to the presence of molten tin (SM+CC+HT500 and BM+SM+CC+HT250 samples) have densities minimally affected by the reference heat treatment cycle performed in the present study.

In general, the density of BM samples takes advantage (increasing) from the addition of SM and HC220 production steps. In BM+CC as produced sample the work hardening promoted during the mixing step, limited the maximum achievable plastic deformation of powders achieved during the compression stage, resulting in lower density than SM+CC+HT500. The absence of sintering above the melting temperature of tin during their production (BM+CC and BM+HC220 samples) experienced slightly higher reduction in the density induced by the reference heat treatment at 250°C. Moreover, the initially low plastic deformability of ball milled powders led to low internal cohesion and to brittle behavior of the as-produced samples.

The development of thermal stresses related to the differences in Al/Sn coefficients of thermal expansions [74,75,78] arisen during the heat treatment cycle which promoted Sn melting and concurrent expansion could have led to inner crack development during healing-focused treatment as shown in Fig. 5b and c and to the flow of Sn, which was able to fill these cracks and to give some surface leakage as well (see Section 3.4).

As far as the liquid metal route samples are concerned, MRS showed a relatively high density, related to the abovementioned porosity (Fig. 5e), which often flanking/staying inside the Sn phase in columnar interdendritic regions. These latter represent a preferential path for Sn mobility and for its exudation to the surface, which is related to the porosity change.

PBLF shows a moderately high porosity, which is significantly affected by the following heat treatment, possibly ascribed to entrapped air or hot cracking, related to the wide solidification range of the Al-Sn system [34,79]. This sample exhibited a certain self-healing potential since the mobile molten Sn was able to fill relatively coarse pores and filled or at least bridged cracks originated during production (see Figs. 5e and 7e). Diffused porosity was in any case left or induced by Sn mobility, and some coarse exudated Sn droplets formed on the free surface (see Section 3.4).

The evaluation of the self-healing potential by the only measurement of density change induced by a potential self-healing heat treatment is not an easy task and it has not been carried out for other potential self-healing heat treatments.

3.4. Quantitative analyses of the exuded Sn

As discussed in Section 3.3, the analysis of sample density and density changes induced by the healing-focused heat treatment with 60 min holding at 250°C was not sufficient to characterize the self-healing potential of the C-PCMs. For this reason, the Al-Sn samples were subjected to a set of five exudation heat treatments, as described in Section 2 in order to stimulate the exudation of the active phase on the specimen surfaces. Indeed, the quantification of the low-melting phase leaked volume was consequently addressed as possible potential self-healing potential indicator, being an estimation of them out of liquid phase that could dislocate and fill the discontinuities formed during service and, consequently, restore thermal conductivity.

This volume was quantified by means of image analysis of Sn exudated droplets, that were considered as perfect spheres, due to the high angle of contact between exuded Sn and the oxidized surface of the samples (Figs. 8, 9 and 13). The average equivalent diameter (d_e) of the droplets and its standard deviation were evaluated from ImageJ results. The results are presented in Fig. 10a and b, comparing the exudation heat treatments performed at different times at 250°C in the former, those at various temperature for 60 min in the latter. The trends in Fig. 10 are various and can be related to the microstructural differences shown in the previous sections. The average diameters related to the samples with the finest microstructures, i.e., BM+CC+HT500, BM+SM+CC+HT250 and PBLF, show quite stable trends with heat treatment time (Fig. 10a) or temperature (Fig. 10b), suggesting minor effect of both heat cycle parameters. The result is coherent with the size of the available Sn basins, which coincides with the limited Sn regions in the microstructures presented in Section 3.2. On the other hand, SM+CC+HT500, BM+HC220 and MRS trends are influenced in a consistent way by the duration and the temperature of the heat treatments (Fig. 10a and b). The results in the graphs below qualitatively reflects the microstructure of SM+CC+HT500, which exhibits extended basins, and BM+HC220, whose Sn is well distributed within the whole matrix. Possibly, in the case of MRS sample, capillary forces in the

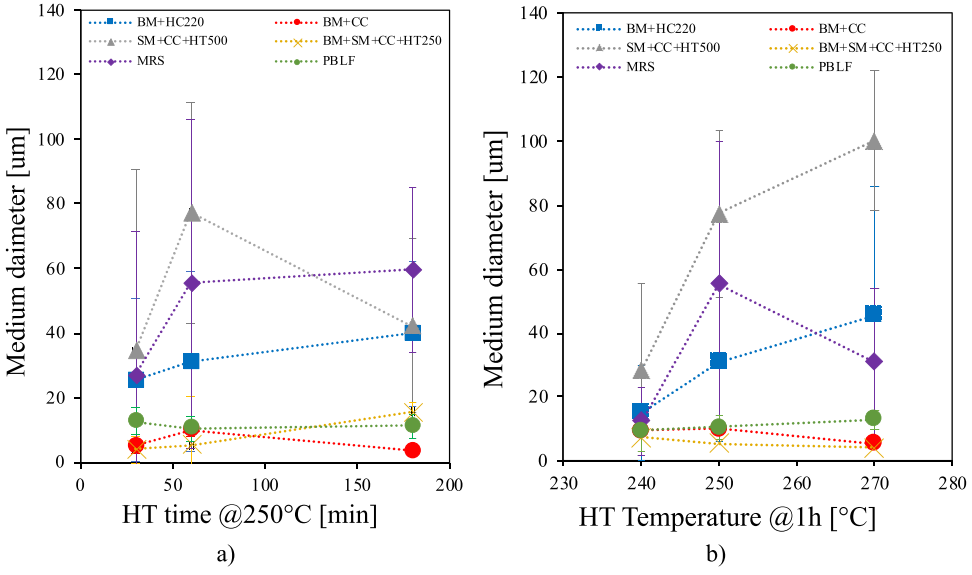

Fig. 10. Trends of the medium diameter of the Sn droplets exuded from the matrix after the heat treatments as a function of (a) holding time @250°C and (b) temperature for 60 minutes holding time.

interdendritic channels, where the oxidation of the Al matrix is less critical [54,55], can act as Sn mobility mechanism, stimulating its leakage. The majority of the collected data suggest an increment in the equivalent diameter as both the heat treatment temperature and holding time increase for the Al-Sn samples with the coarser Sn regions, i.e., MRS and SM+CC+HT500. However, some points deviate from the suggested trend for these latter, even considering the relatively large standard deviation values. The local presence of signs of detachment (Fig. 9c) suggests that some of the largest droplets formed on the surface of these C-PCM in the most critical conditions have then been detached from the surface due to the weak interaction between the exuded solidifying Sn, which experiences shrinkage forces, and the oxidized Al surface, possibly enhanced by the handling of the samples. On the other hand, heat treatment temperatures and holding time have a much more limited incidence on the results of the remaining structures, which exhibit much finer microstructures.

The total amount of Sn exuded on the sample surface was quantified computing the percentage of the covered area as the ratio between the sum of the areas of all the Sn leaked droplets with respect and the total area of the micrographs (Eq. (2)):

$$Percentage\ \ of\ \ covered\ \ area\ \ (\%) = \frac{\sum Area\ \ of\ \ Sn\ \ droplets}{Total\ \ area\ \ of\ \ the\ \ micrograph} * 100 \quad (2)$$

Summaries of the trends of this Sn mobility index for various C-PCMs are given in term of heat treatment time and temperature in Fig. 11a and b, respectively. With respect to all other samples investigated, BM+CC exhibits the lowest percentage of covered area with a general slight effect of heat treatment parameters. Time and temperature trends like the one of the average diameters can be observed for both SM+CC+HT500 and MRS Al-Sn. Notwithstanding the small average diameter of the exuded Sn, the highest values of the covered area belong to the PBLM specimens, due to the presence of many droplets having small equivalent diameter together with some bigger ones, possibly due to the high percentage of discontinuities as testified by both micrographic analyses, clearly visible in Figs. 4f and 6f, and density measurements, Table 2. These latter are related to the flow and exudation of Sn through the cracks related to the production process itself (Fig. 5f), whose thicknesses can reach also a tenth of micrometers.

A second index was derived from quantitative metallography results to evaluate Sn mobility: the total volume of the exudated Sn (V_t, Eq. (3)).

$$V_t = \sum \frac{4}{3}\pi\left(\frac{d_e}{2}\right)^3 \quad (3)$$

This was evaluated considering that Sn droplets as spheres, i.e., fulfilling a complete non-wetting condition. This situation is close to that demonstrated by in-situ CT scans of SM+CC+HT500 during heat treatment cycle [73], and was observed in a big exuded droplet from cross-sectioned MRS sample (Fig. 12), where the superficial Al oxide prevents the contact with the exuded Sn. The almost spherical shape of the Sn droplets is also suggested for various samples by their surface micrographs in Figs. 8 and 9. Under this assumption, the estimated volume of droplets is the maximum possible for the 2D measured equivalent diameter of the droplets. Droplets surface depressions and possible changes of the contact angle between molten Sn and the sample surface were considered to have small effect on the so-derived total volume of exudated tin.

The total volume of exudated Sn was the basis for the calculation of a third and more significant index in view a rough estimation of the self-healing potential of the system: the coverable thickness (t) which is the thickness that can be uniformly coated by Sn exudated on a free surface. This was calculated considering as the ratio between the volume exudated Sn and the total surface area of the micrographs used for quantitative analyses (A), as in the following Eq. (4):

$$t = 2\frac{Vt}{A} \quad (4)$$

It should be here mentioned that the t-parameter does not correspond to the distance between surfaces of a crack that can be completely filled by the exudated Sn. This latter, also referred as fillable crack thickness, is twice the coverable thickness since Sn exudates from the two surfaces of the crack. Nevertheless, also considering this point, the coverable thickness can be considered as the index of self-healing potential.

The values of t calculated by the above equation are here presented in Fig. 13 for the analyzed samples, arranged as usual, to display the effects of holding time at 250°C (Fig. 13a) and test temperature for holding time of 60 min (Fig. 13b). The highest values of the t index are obtained by the materials produced by "liquid metal route" and for SM+CC+HT500, BM+HC220 samples for the classes of "powder metallurgy route", coherently with what shown in Fig. 11. In general, it is possible to conclude that these microstructures grant the highest Sn

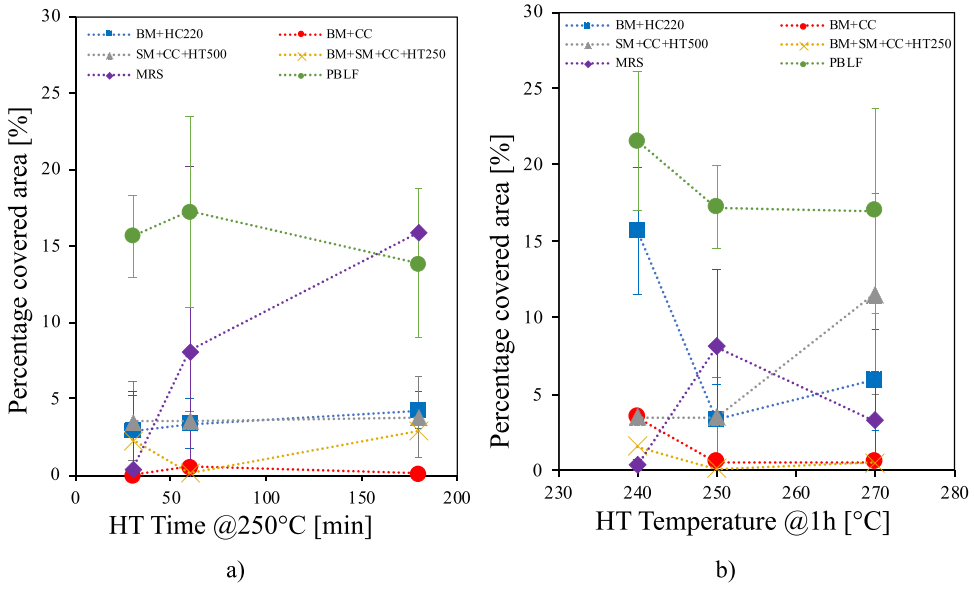

Fig. 11. Trends related to the percentage of area covered by the Sn exited from the composite system as a function of the holding time @250°C (a) and the temperature for 60 minutes holding time (b).

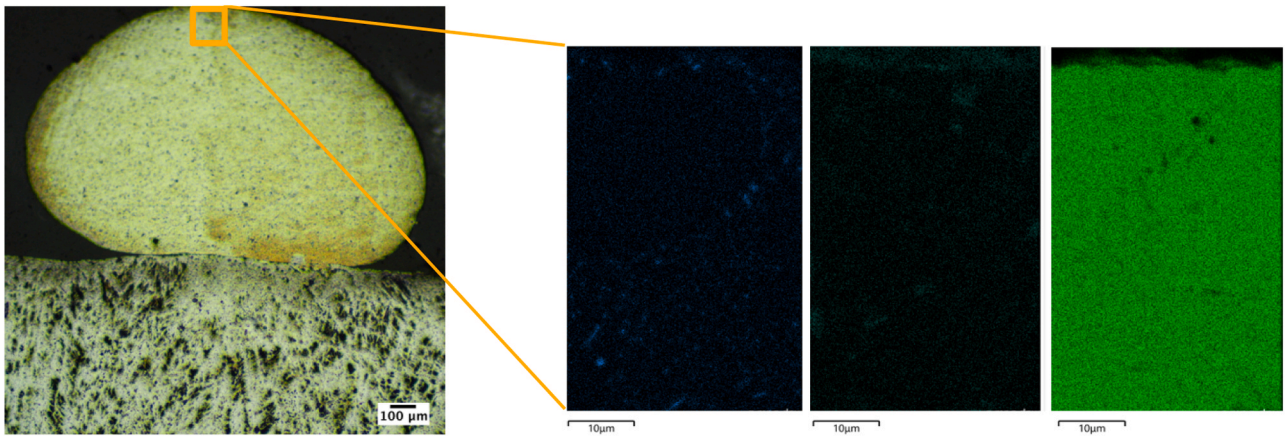

Fig. 12. 100x magnification micrograph of exuded Sn on the heat treated MRS C-PCM surface heat treated for 1 h at 250°C, whose bulk region appear depleted. EDS maps of the leaked Sn are presented. From left to right: Al, O_2 and Sn.

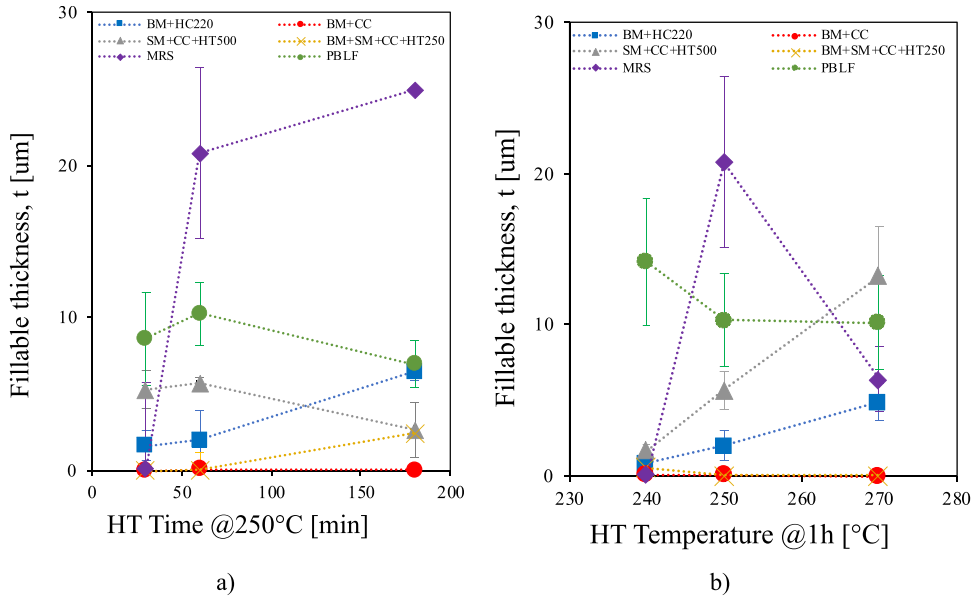

Fig. 13. Trends of the self-healing potential index after the heat treatment as a function of the holding time @250°C (a) and the temperature for 60 minutes holding (b).

mobility, as assessed by its exuded quantities (Figs. 10, 11 and 13) and, consequently, show the highest self-healing potential index *t*, coherently with the microstructural observation. In all cases, the calculated thickness *t* only occasionally reaches values greater than 20 µm. On the other hand, the coverable thickness of the Al-Sn systems with finer microstructures slightly increases with heat treatment time or temperature, remaining in any case below the 6 µm also.

The results regarding the thickness of the fillable discontinuity are coherent with what shown in the micrographs in Fig. 7b, c and f where the crack is locally replenished by the low-melting phase. The quantitative analyses on the exuded Sn results underline the importance of the technology selection for the production of Al-Sn PCM and self-healing systems. As far as the powder metallurgy route is concerned, self-healing potential seems to be favored by larger Sn areas (SM+CC+HT500 offers higher *t*). In this sense, the control of the powders size seems to be crucial, as well as avoiding the ball milling, that leads to too small microstructural features. In the same way, cooling rates imposed during the solidification stage seems to be strictly correlated to *t*. However, the high mobility offered by this type of microstructure should be carefully controlled in order to limit excessive leak of the active phase, which can in turn lower both the PCM and the self-healing performances.

3.5. EDS analyses of exuded Sn

The effect of temperature and time of heat treatment on the chemical composition of exudated droplets of Sn-rich phase has been analyzed for SM+CC+HT500, BM+CC, MRS and PBLF samples, considered as representative of the more and less promising systems in terms of self-healing potential. The chemical composition from EDS analyses of Sn-rich phase in as produced sample and at the external (upper) surface of droplets exudated during various heat treatments are compared in Fig. 14 in terms of Al content (mass %). The aim was to quantify Al release or dissolution promoted by the molten Sn phase mobility, investigating on the Sn mobility mechanism.

In the examined samples, temperature and time differently influence the Al content in Sn droplets with respect to the initial Sn-rich phase. In the as produced condition, the considered SM+CC+HT500 exhibited Al contents higher than the equilibrium value at room temperature of 0.432% [62]. Higher Al content has been detected on both MRS and

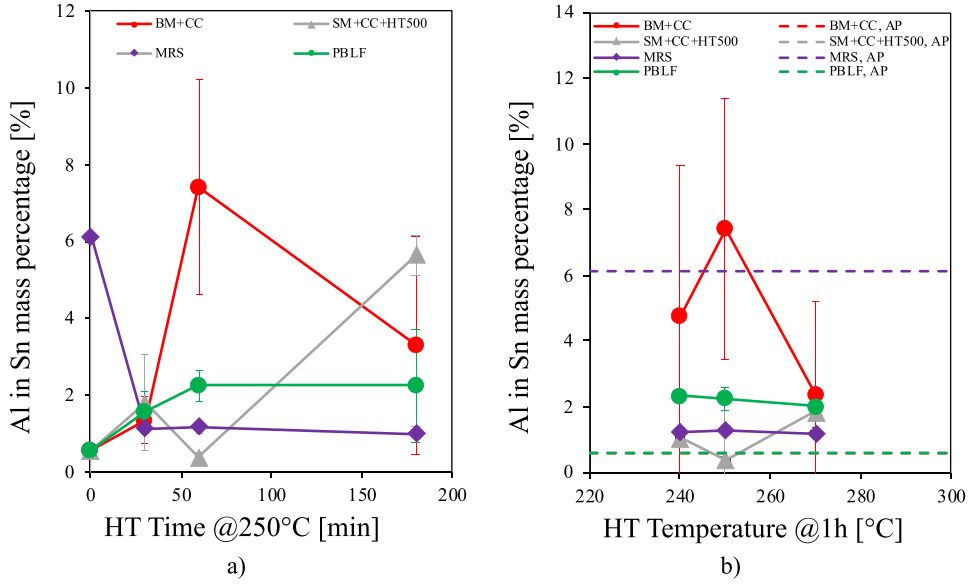

Fig. 14. Effect of time spent at 250°C (a) and of test temperature for 60 minutes heat treatment duration (b) on the Al content in Sn phase. In Fig. 11b the dashed lines are referred to the as produced values.

PBLF samples in which the high solidification and cooling rate, led to Al entrapment in Sn-solid solution. The application of heat treatments on the samples favors the competition of different processes in the Sn-rich phases: (i) the tendency of entrapped Sn to eject Al to reach the equilibrium values at the heat treatment temperature, (ii) Al dissolution in liquid Sn and re-deposition, promoted either by chemical activity gradients or thermal stresses at the interface of the two phases, [68,72,80], (iii) Al tendency to move upward in the molten phase due to gravimetric reasons (iv) Al and Sn tendency to form oxides at the droplet surface even in the presence of oxygen traces.

As far as the powder metallurgy samples are concerned, an increasing trend with the increment of time can be observed from Fig. 14a and b, which stabilize in the longer heat treatment conditions. Conversely, higher temperatures seem to favor Al ejection from Sn-rich phases for equilibrium reasons (its equilibrium content increases from 0.273% to 0.424% at 240°C and 270°C with respect to room temperature conditions [62], respectively). In the case of the materials produced by ball milling, it should be highlighted that the small size (and bigger surface curvature) of the droplets exudated from a fine microstructure could be responsible not only of the high data scatter in Al content, but possibly, of the high measured Al content. Conversely, holding at higher temperatures and longer times samples produced via liquid metal route (MRS and PBLF) promotes a slight decrease in the Al content with respect to supersaturated solid solutions in Al of the as-produced conditions.

The highly scattered Al content values suggest a non-homogeneous development of the Al dissolution in Sn process, being related to surface energies [66,67]. In this sense, different grain boundary orientations promote different dissolution kinetics. It is also important to highlight that smaller Sn basins, as in the case of BM+CC and PBLF samples, can generally lead to a faster Al dissolution, possibly due to most severe chemical activity special gradients.

3.6. *Thermal diffusivity and functional self-healing considerations*

As discussed in Section 2, the functional self-healing feature of the examined Al-Sn alloys was tested by LFA analyses, addressed toward the estimation of the thermal diffusivity of the samples before (As produced condition, AP) and after the reference heat treatment at 250°C for 60 minutes, considered as potential healing-focused cycle (H). On the bases of the choices depicted in the previous chapter, BM+CC, MRS, PBLF and SM+CC+HT500 were subjected, after healing-focused heat treatment, to further ten simulated service heat treatments between 170 and 270°C (H+10 S) plus another healing cycle (H+10 S+H). Fig. 15 presents, for the investigated production techniques, thermal diffusivity data of as-produced, healing-treated, simulated serviced and further healing treated samples. The analyzed data are averaged when 2 samples per material and condition are available. Fig. 15 highlights that as produced thermal diffusivity is clustered around two values: samples processed from metallic powder that did not undergo high temperature treatment show values around 0.2 cm^2/s while sample from molten route and simple mixed that has been treated at 500°C present values in the range of 0.5–0.6 cm^2/s. This difference can be ascribed to the presence in the latters of a continuous Al network, whilst the others are characterized by an extremely fine microstructure and discontinuities.

The comparison between as produced and healed samples exhibit for these latter a slight gain in thermal diffusivity for all the studied cases, with the only exception of BM+SM+CC+HT250 sample, where thermal diffusivity diminishes by approximately 2% with respect to the as-produced condition.

However, its thermal diffusivity can be considered practically constant if the data scatter is taken into account, i.e., thermal diffusivity values remain in the standard deviation.

The results are coherent with the microstructural observations in Section 3.1. and 3.2., where minimal feature changes and absence of

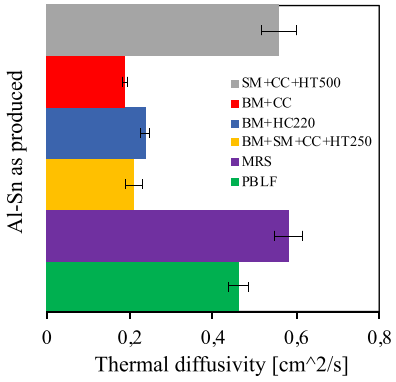

Fig. 15. Thermal diffusivity evaluated in the as produced samples.

damages are exhibited between the as produced and the healed conditions, as well as with slight density difference changes (Section 3.3.). Moreover, minimal compositional changes are expected between the as produced and the healing focused heat-treated sample due to HT stage in the production stage of the C-PCM, which should have led both Al and Sn phases toward the equilibrium composition. The previous chapters suggest its microstructure to be stable, at least after the healing focused heat treatment. On the other hand, in sample BM+HC220 (blue bars in Fig. 15), a partial modification of the solute atoms content of phases may have occurred during material processing as the ball-milled powders were kept at 220°C during the compression step, with a concurrent tendency toward stable phase compositions. Thus, healing-focused heat treatment offers a slight increment of thermal diffusivity, i.e., approximately 1%, induced by the crack filling (Table 3).

For SM+CC+HT500, BM+CC, MRS and PBLF samples thermal diffusivity data in the as produced condition have been further compared to those after simulated service (H+10 S) and after a further healing cycle (H+10 S+H) in Table 3.

The thermal diffusivity remains practically unchanged after healing treatment (the relative difference is around 1%) in the case of SM+CC+HT500 (gray bars in Fig. 15), the sample which displayed moderate healing index *t,* and in which Sn exuded only from the relatively coarse surface Sn regions [60]. As mentioned in Section 3.1, the sintering above the melting temperature of tin has induced Sn-mobility and redistribution during the production step and no significant changes are induced by the healing-focused heat treatment selected here to prove healing potential, as witnessed by both the qualitative minimal changes detected in microstructure and in the porosity content.

After simulated service cycles where the maximum temperature slightly overcome the healing one, the expected compositional changes of phases are minimal. This agrees with the good microstructural stability observed by [58] on these material after 100 simulated cycles without intermediate healing-focused treatment. The small compositional changes occurred during the first healing-focused treatment could have progressed concurrently to the simulated service, leading to slight increase of the thermal conductivity (approximately 3%). The second healing focused heat treatment led thermal diffusivity practically unaltered (a loss of 0.268% was quantified), further testifying the stability of the C-PCM.

BM+CC (red bars in Fig. 15) showed the highest increase of the thermal diffusivity (8%) between the as produced and the healed condition, notwithstanding moderate density reduction and the absence of microstructural changes. This could be related to the positive crack filling effect due to the small but effective mobility of molten Sn, showed by Fig. 7b and discussed in Section 3.4. A concurrent effect could have in any case contributed to thermal diffusivity gain: holding at temperature of 250°C has favored phase composition adjustment toward equilibrium, with corresponding increase of thermal conductivity, mitigating the effects of the possible mechanical alloying, encountered in the production phase. Indeed, mechanical alloying action could have brought about some degree of supersaturation in both Al- and Sn- finely dispersed phases which is known to reduce thermal conductivity (and diffusivity) [81]. BM+CC experiences a reduction in thermal diffusivity (-5% with respect to the healed condition) after the simulated service possibly related to thermal fatigue phenomena related to Al and Sn CTE mismatches [75,78] that may have led to crack opening in the composite. However, the consequent healing treatment allows to recover a further 2.5% in thermal diffusivity. Possibly, the holding time at 250°C let molten Sn to move inside Al matrix and promote bridging. A similar situation could potentially occur in C-PCM when their service cycle includes relatively long periods above the melting temperature of the molten phase.

Table 3
Thermal diffusivity relative differences, evaluated after healing treatment (250°C, 1 hour), 10 simulated service cycles and a further healing treatment with respect to the as produced condition.

Thermal diffusivity relative difference with respect to AP [%]	Healed	Healed + 10 simulated service	Healed + 10 simulated service + healed
SM+CC+HT500	1.092 ± 0.256	3.172 ± 0.558	2.904 ± 0.519
BM+CC	8.52 ± 0.93	-4.975 ± 0.569	2.525 ± 0.127
BM+HC220	0.911 ± 2.43	Not performed	Not performed
BM+SM+CC+HT250	-1.901 ± 1.579	Not performed	Not performed
MRS	5.59 ± 0.811	4.502 ± 0.872	5.783 ± 0.831
PBLF	2.26 ± 0.13	-5.767 ± 0.703	-4.495 ± 0.211

The attention will be now focused on the two samples produced by the liquid metal route: MRS and PBLF. Concerning MRS sample, the measured thermal diffusivity increases of about 6% after healing-focused treatment, taking advantage both from the microstructural rearrangement and phases composition modification promoted by the heat treatment above the Sn melting temperature, shown in Section 3.2. Actually in the heat treated condition the high conductivity and high diffusivity Al phase forms a continuous network around globular Sn inclusions, the most suitable situation in terms of thermal conductivity for a fully dense composite structure made of an high and a low-conductivity phase [19]. In the present case, also considering the reduction in the porosity induced by healing-focused t treatment, the functional recovery is quite good. The functional healing effect in terms of thermal conductivity gain cannot be directly correlated to the good quantitative self-healing indexes such as t. As a matter of fact, these latter have been obtained based on exudated Sn on the free surface of the sample during the exudation heat treatment that was concurrently modifying the inner microstructure of the material, from a columnar structure favoring Sn mobility to a globular distribution of Sn inclusions, hardly interconnected. Minor effects were probably played by small compositional changes of the phases, as demonstrated by EDS analyses, at least on exudated droplets (Section 3.5). The further simulated service left substantially unaltered the thermal conductivity of the healed condition, with a reduction of approximately 6%, possibly due to an uncontrolled Sn movement. Thermal diffusivity experience 1% gain after the second healing treatment with respect to the serviced condition. This could be potentially a result of the rather stable microstructure induced by healing-focused thermal cycle. Also in this case the presence of fully molten Sn phase during service for relatively long time could be beneficial for functional healing.

The relative increase of thermal diffusivity of PBLF healed sample with respect to the as-produced one was of about 4%. With respect to MRS C-PCM, during PBLF processing the material locally experienced high solidification rates, but these were followed by healed-focused cycle, which left the Al content in Sn (and viceversa) relatively close to equilibrium values. The composition of both phases was then relatively stable during simulated-service heat treatment, with minimal effects on the thermal conductivity improvement obtained on the healed or simulated serviced PBLF sample in view of functional self-healing. Under the conditions of stable microstructure, chemical composition of phases and porosity, the Sn exudation characteristics define healing functionality of the sample. There, high thickness coverage index *t* is able to predict the partial filling of both the process-related relatively wide cracks present in the as produced sample and the ones developed during the healing thermal treatments (Fig. 7f), in both cases partly emerging to the surface and exudating Sn during heat treatment. This situation was also observed on the sample further subjected to simulated cycles, which thermal diffusivity diminished, possibly due to uncontrolled Sn movement outside the composite. The subsequent healing focused treatment, whose holding time let Sn to move inside the fine matrix, allows a partial recovery in terms of thermal diffusivity. The

relative importance of Sn exudation on thermal diffusivity could be expected to become lower in PBLF components characterized by lower surface to volume ratio than the LFA samples, with beneficial effects.

From the above analyses, heat treatments in the upper range of service conditions and relatively long times demonstrate to be often beneficial in recovering heat diffusivity of damaged C-PCMs. The analyses of thermal diffusivity, in the light of microstructural features and chemical composition variations of the phases suggests that the functional recovery of thermal conductivity and diffusivity is not only related to the flowability of the low-melting Sn phase towards cracks or porosity, but it is also affected by microstructure and phase composition content. The self-healing potentials based on the quantitative analyses are strictly correlated to the increase of thermal diffusivity (and conductivity) if stable microstructure and phase compositions are observed (ex. SM+CC+HT500). Samples in which the processing route promotes unstable microstructures or non-equilibrium phase composition (MRS, PBLF and BM+CC, for example) can benefit of the heat treatment with functional healing purposes as a final step in their production, before they are put in service, to obtain Al-Sn C-PCMs with higher diffusivity. As previously suggested, as far as powder metallurgy samples are concerned, the use of powders with higher sizes, without ball milled operations, may lead to higher self-potential and promote at the same time more stable microstructure which benefits from heat treatments in terms of thermal diffusivity. On the other hand, both the examined liquid metal techniques offer Al-Sn systems with high healing potential, but the instability of their microstructure may threaten their thermal diffusivity performances, mainly in PBLF. Further analyses are planned by the authors on samples exhibiting improved thermal diffusivity by healing-focused thermal cycles or simulated service to investigate the possibility to have self-healing directly induced by service conditions or to adopt a healing-focused treatment preliminary to the service of C-PCM Al-Sn composite.

4. Conclusions

A preliminary campaign of tests for evaluating self-healing potential on C-PCM Al-Sn systems successfully produced for thermal management purposes via either powder metallurgy or liquid metal routes was performed. The aim of the study was to understand the feasibility of obtaining multi-functional metallic composite phase change materials systems, combining thermal energy storage with functional self-healing features, and setting the microstructural requirements to develop them. A set of heat treatments was performed on the selected samples to establish their self-healing potential, evaluated from the quantification of the Sn exuded from the surfaces of internal sections of the samples. EDS analyses were performed as well on the leaked low-melting Sn to investigate its mobility mechanism in the composite. Thermal diffusivity tests were performed on the selected samples, before and heat treatment 250°C for 60 minutes heat treatment, to verify the effective healing capability of the low-melting phase of the C-PCM, i.e., Sn. Service was simulated by heat treatment cycles following the healing-focused thermal cycle. The results of the study can be summarized as follows:

- BM+CC and BM+SM+CC+HT250 samples, characterized by a refined microstructure, present limited Sn basins, resulting in a limited exudation of the low-melting phase and consequently, restrained self-healing potential. Notwithstanding the fine microstructure instead, PBLF Al-Sn exhibits consistent healing potential, possibly favored by the cracks network formed during production. On the other hand, the extended Sn areas of the remaining powder metallurgy samples, i.e., SM+CC+HT500 and BM+HC220, offer copious leakage, which can easily move inside the composite when molten. Also, MRS sample shows relevant potential, with extended available Sn basins coinciding with interdendritic channels that progressively get deplenished of healing agent by capillary action.
- EDS analyses performed on the leaked Sn reveal the presence of Al in the molten and solidified low-melting phase. Its quantity depends on the amount of Al dissolved under the effect of heat treatment temperature and holding time and its ejection from Sn-rich phases promoted by thermodynamic equilibrium reasons. The authors believe that, in addition to Sn flowing in the composite discontinuities (Fig. 5b, c and f), the low-melting phase move across in the matrix by Al dissolution and redeposition. In the MRS sample, a microstructural rearrangement occurs, governed by Rayleigh's instability which leads to the spheroidization of interdendritic Sn regions.
- Density measurements, performed on Al-Sn samples in as produced and healed conditions, are not a reliable tool for the estimation of the functional self-healing potential of the Al-Sn alloys.
- The functional recovery of thermal diffusivity induced by healing-focused het heat cycle analyzed via LFA tests results demonstrate the presence of molten Sn in the proposed system is potentially beneficial for thermal diffusivity recovery, especially for damaged samples, since it promoted bridging capability, verified with metallographic investigations. Nevertheless, thermal diffusivity changes are not only related to Sn mobility, but also by compositional, microstructural changes and Sn exudation from sample surfaces. The analyses of the overall situation is quite complex, and partly related to material geometry (surface to volume ratio).
- The stability of thermal diffusivity during relatively small simulated service cycle, performed in a temperature range including the healing-focused treatments, is affected by the abovementioned effects. The beneficial role of healing focused heat treatments at 250°C for 1 hour suggests that the presence of fully molten Sn phase during service for relatively long time could be beneficial for functional healing.

BM+CC, notwithstanding its limited healing potential, and SM+CC+HT500 structures experienced high thermal diffusivity recovery performing healing focused treatments. However, the integrity of the microstructure of the former, which gets easily damaged, threaten the performances of the C-PCM. Despite the high healing potential, liquid metal route samples show ambiguous trends in terms of thermal diffusivity recovery.

In the latter case, further analyses will be performed to check the investigated functional self-healing capability directly during service life.

CRediT authorship contribution statement

Matteo Molteni: Investigation, Visualization, Writing – original draft, Writing – review & editing. **Antonio Mattia Grande:** Conceptualization, Methodology, Writing – original draft, Writing – review & editing. **Elisabetta Gariboldi:** Conceptualization, Methodology, Writing – original draft, Writing – review & editing. **Paola Bassani:** Conceptualization, Methodology, Writing – original draft, Writing – review & editing.

Declaration of Competing Interest

The authors declare that they have no known competing financial interests or personal relationships that could have appeared to influence the work reported in this paper

Data availability

The authors do not have permission to share data.

Acknowledgments

The authors would like to thank for their valuable work Mr. Luca Nemboli and Dr. Chiara Confalonieri-Polimi.

The authors acknowledge the Italian Ministry of Education, University and Research for the support through the Project "Department of Excellence LIS4.0–Lightweight and Smart Structures for Industry 4.0", and partial support through the Ph.D. grant "Multi-functional Metallic and Hybrid Materials", funded on ESF-REACT EU resources (Ministerial Decree 1061/2021) from the National Operational Plan Research and Innovation 2014–2020 – Action IV.5 (PhDs on Green Themes).

References

[1] I. Sarbu, A. Dorca, Review on heat transfer analysis in thermal energy storage using latent heat storage systems and phase change materials, Int. J. Energy Res. 43 (2019) 29–64, https://doi.org/10.1002/er.4196.
[2] P.H. Feng, B.C. Zhao, R.Z. Wang, Thermophysical heat storage for cooling, heating, and power generation: a review, Appl. Therm. Eng. 166 (2020) 114728, https://doi.org/10.1016/j.applthermaleng.2019.114728.
[3] A. Sharma, V.V. Tyagi, C.R. Chen, D. Buddhi, Review on thermal energy storage with phase change materials and applications, Renew. Sustain. Energy Rev. 13 (2009) 318–345, https://doi.org/10.1016/j.rser.2007.10.005.
[4] K. Pielichowska, K. Pielichowski, Phase change materials for thermal energy storage, Prog. Mater. Sci. 65 (2014) 67–123, https://doi.org/10.1016/j.pmatsci.2014.03.005.
[5] P.J. Shamberger, N.M. Bruno, Review of metallic phase change materials for high heat flux transient thermal management applications, Appl. Energy 258 (2020) 113955, https://doi.org/10.1016/j.apenergy.2019.113955.
[6] T. Fiedler, A.J. Rawson, H. Sugo, E. Kisi, Thermal capacitors made from miscibility gap alloys (MGAs), WIT Trans. Ecol. Environ. 186 (2014) 479–486, https://doi.org/10.2495/ESUS140411.
[7] S.C. Costa, M. Kenisarin, A review of metallic materials for latent heat thermal energy storage: thermophysical properties, applications, and challenges, Renew. Sustain. Energy Rev. 154 (2022) 111812, https://doi.org/10.1016/j.rser.2021.111812.
[8] Y. Zhao, C.Y. Zhao, C.N. Markides, H. Wang, W. Li, Medium- and high-temperature latent and thermochemical heat storage using metals and metallic compounds as heat storage media: a technical review, Appl. Energy 280 (2020), https://doi.org/10.1016/j.apenergy.2020.115950.
[9] P.J. Shamberger, N.M. Bruno, Review of metallic phase change materials for high heat flux transient thermal management applications, Appl. Energy 258 (2020) 113955, https://doi.org/10.1016/j.apenergy.2019.113955.
[10] J. Nieto-Maestre, I. Iparraguirre-Torres, Z.A. Velasco, I. Kaltzakorta, M.M. Zubieta, Novel metallic alloys as phase change materials for heat storage in direct steam generation applications, AIP Conf. Proc., 1734, 2016, https://doi.org/10.1063/1.4949130.
[11] A.I. Fernández, C. Barreneche, M. Belusko, M. Segarra, F. Bruno, L.F. Cabeza, Considerations for the use of metal alloys as phase change materials for high temperature applications, Sol. Energy Mater. Sol. Cells 171 (2017) 275–281, https://doi.org/10.1016/j.solmat.2017.06.054.
[12] A.K. Ray, D. Rakshit, K. Ravikumar, High-temperature latent thermal storage system for solar power: materials, concepts, and challenges, Clean. Eng. Technol. 4 (2021) 100155, https://doi.org/10.1016/j.clet.2021.100155.
[13] F.S. Javadi, H.S.C. Metselaar, P. Ganesan, Performance improvement of solar thermal systems integrated with phase change materials (PCM), a review, Sol. Energy 206 (2020) 330–352, https://doi.org/10.1016/j.solener.2020.05.106.
[14] W. Lee, J. Lee, W. Kyoung, H. Lee, H. Lee, D. Kim, Effect of inhomogeneous composition on the thermal conductivity of an Al alloy during the precipitation-hardening process, J. Mater. Res. Technol. 9 (2020) 10139–10147, https://doi.org/10.1016/j.jmrt.2020.07.040.
[15] R. Fukahori, T. Nomura, C. Zhu, N. Sheng, N. Okinaka, T. Akiyama, Macro-encapsulation of metallic phase change material using cylindrical-type ceramic containers for high-temperature thermal energy storage, Appl. Energy 170 (2016) 324–328, https://doi.org/10.1016/j.apenergy.2016.02.106.
[16] S. Zhu, M.T. Nguyen, T. Yonezawa, Micro- And nano-encapsulated metal and alloy-based phase-change materials for thermal energy storage, Nanoscale Adv. 3 (2021) 4626–4645, https://doi.org/10.1039/d0na01008a.
[17] A. Dindi, N. Lopez Ferber, D. Gloss, E. Rilby, N. Calvet, Compatibility of an Aluminium-Silicon metal alloy-based phase change material with coated stainless-steel containers, J. Energy Storage 32 (2020) 1–18, https://doi.org/10.1016/j.est.2020.101961.
[18] A. Rawson, C. Villada, M. Kolbe, V. Stahl, F. Kargl, Suitability of aluminium copper silicon eutectic as a phase change material for thermal storage applications: thermophysical properties and compatibility, Energy Storage 4 (2022) 1–15, https://doi.org/10.1002/est2.299.
[19] H. Sugo, E. Kisi, D. Cuskelly, Miscibility gap alloys with inverse microstructures and high thermal conductivity for high energy density thermal storage applications, Appl. Therm. Eng. 51 (2013) 1345–1350, https://doi.org/10.1016/j.applthermaleng.2012.11.029.
[20] N.K. Guimard, K.K. Oehlenschlaeger, J. Zhou, S. Hilf, F.G. Schmidt, C. Barner-Kowollik, Current trends in the field of self-healing materials, Macromol. Chem. Phys. 213 (2012) 131–143.
[21] S. Utrera-Barrios, R. Verdejo, M.A. López-Manchado, M. Hernández Santana, Evolution of self-healing elastomers, from extrinsic to combined intrinsic mechanisms: a review, Mater. Horiz. 7 (2020) 2882–2902, https://doi.org/10.1039/d0mh00535e.
[22] S.R.M. Paladugu, P.S.R. Sreekanth, S.K. Sahu, K. Naresh, S.A. Karthick, N. Venkateshwaran, M. Ramoni, R.A. Mensah, O. Das, R. Shanmugam, A comprehensive review of self-healing polymer, metal, and ceramic matrix composites and their modeling aspects for aerospace applications, Materials 15 (2022), https://doi.org/10.3390/ma15238521.
[23] J.T. Kim, H.J. Kim, S.H. Hong, H.J. Park, Y.S. Kim, Y.J. Hwang, Y.B. Jeong, J. Y. Park, J.M. Park, B. Sarac, W.M. Wang, J. Eckert, K.B. Kim, Thermally-triggered dual in-situ self-healing metallic materials, Sci. Rep. 8 (2018) 2–11, https://doi.org/10.1038/s41598-018-19936-4.
[24] H. Yu, Y. Feng, L. Gao, C. Chen, Z. Zhang, W. Feng, Self-healing high strength and thermal conductivity of 3D graphene/PDMS composites by the optimization of multiple molecular interactions, Macromolecules 53 (2020) 7161–7170, https://doi.org/10.1021/acs.macromol.9b02544.
[25] Z. Shang, D. Ding, X. Wang, B. Liu, Y. Chen, L. Gong, Z. Liu, Q. Zhang, High thermal conductivity of self-healing polydimethylsiloxane elastomer composites by the orientation of boron nitride nano sheets, Polym. Adv. Technol. 32 (2021) 4745–4754, https://doi.org/10.1002/pat.5467.
[26] F. Chen, H. Xiao, Z.Q. Peng, Z.P. Zhang, M.Z. Rong, M.Q. Zhang, Thermally conductive glass fiber reinforced epoxy composites with intrinsic self-healing capability, Adv. Compos. Hybrid Mater. 4 (2021) 1048–1058, https://doi.org/10.1007/s42114-021-00303-3.
[27] H. Yu, C. Chen, J. Sun, H. Zhang, Y. Feng, M. Qin, W. Feng, Highly thermally conductive polymer/graphene composites with rapid room-temperature self-healing capacity, Nano-Micro Lett. 14 (1) (2022) 14, https://doi.org/10.1007/s40820-022-00882-w.
[28] D.W. Yue, H.Q. Wang, H.Q. Tao, P. Zheng, C.H. Li, J.L. Zuo, A fast and room-temperature self-healing thermal conductive polymer composite, Chin. J. Polym. Sci. (Engl. Ed.) 39 (2021) 1328–1336, https://doi.org/10.1007/s10118-021-2620-1.
[29] X. Lü, H. Tang, H. Wang, X. Meng, F. Li, Ultra-soft thermal self-healing liquid-metal-foamed composite with high thermal conductivity, Compos. Sci. Technol. 226 (2022) 109523, https://doi.org/10.1016/j.compscitech.2022.109523.
[30] Q. Zhang, L. Liu, C. Pan, D. Li, Review of recent achievements in self-healing conductive materials and their applications, J. Mater. Sci. 53 (2018) 27–46, https://doi.org/10.1007/s10853-017-1388-8.
[31] Y. Xin, H. Peng, J. Xu, J. Zhang, Ultrauniform embedded liquid metal in sulfur polymers for recyclable, conductive, and self-healable materials, Adv. Funct. Mater. 29 (2019), https://doi.org/10.1002/adfm.201808989.
[32] J.B. Ferguson, B.F. Schultz, P.K. Rohatgi, Self-healing metals and metal matrix composites, JOM 66 (2014) 866–871, https://doi.org/10.1007/s11837-014-0912-4.
[33] B.J. Blaiszik, S.L.B. Kramer, M.E. Grady, D.A. McIlroy, J.S. Moore, N.R. Sottos, S. R. White, Autonomic restoration of electrical conductivity, Adv. Mater. 24 (2012) 398–401, https://doi.org/10.1002/adma.201102888.
[34] A.J. McAlister, D.J. Kahan, The Al-Sn (aluminum-tin) system, Bull. Alloy Phase Diagr. 4 (1983) 410–414.
[35] Thermo-calc, Thermo-Calc Documentation Set Thermo-Calc Version 2023a, (n.d.). ⟨https://thermocalc.com/support/documentation/⟩ (Accessed 21 January 2023).
[36] A. Kroupa, Modelling of phase diagrams and thermodynamic properties using Calphad method - development of thermodynamic databases, Comput. Mater. Sci. 66 (2013) 3–13, https://doi.org/10.1016/j.commatsci.2012.02.003.
[37] T. Marrocco, L.C. Driver, S.J. Harris, D.G. McCartney, Microstructure and properties of thermally sprayed Al-Sn-based alloys for plain bearing applications, J. Therm. Spray Technol. 15 (2006) 634–639, https://doi.org/10.1361/105996306×147009.
[38] X. Liu, M.Q. Zeng, Y. Ma, M. Zhu, Promoting the high load-carrying capability of Al–20wt%Sn bearing alloys through creating nanocomposite structure by mechanical alloying, 387–394, Wear (2012) 294–295, https://doi.org/10.1016/j.wear.2012.07.021.
[39] M.E. Makhatha, O.S. Fatoba, E.T. Akinlabi, Effects of rapid solidification on the microstructure and surface analyses of laser-deposited Al-Sn coatings on AISI 1015 steel, Int. J. Adv. Manuf. Technol. 94 (2018) 773–787, https://doi.org/10.1007/s00170-017-0876-y.
[40] T. Stuczyński, Metallurgical problems associated with the production of aluminium-tin alloys, Mater. Des. 18 (1997) 369–372, https://doi.org/10.1016/s0261-3069(97)00078-2.
[41] M.C. Lucchetta, F. Saporiti, F. Audebert, Improvement of surface properties of an Al–Sn–Cu plain bearing alloy produced by rapid solidification, J. Alloy. Compd. 805 (2019) 709–717, https://doi.org/10.1016/j.jallcom.2019.07.082.
[42] N.A. Belov, T.K. Akopyan, I.S. Gershman, O.O. Stolyarova, A.O. Yakovleva, Effect of Si and Cu additions on the phase composition, microstructure and properties of Al-Sn alloys, J. Alloy. Compd. 695 (2017) 2730–2739, https://doi.org/10.1016/j.jallcom.2016.11.193.
[43] C. Confalonieri, A.T. Grimaldi, E. Gariboldi, Ball-milled Al–Sn alloy as composite Phase Change Material, Mater. Today Energy 17 (2020) 100456, https://doi.org/10.1016/j.mtener.2020.100456.
[44] C. Confalonieri, E. Gariboldi, Combined powder metallurgy routes to improve thermal and mechanical response of Al−Sn composite phase change materials, Trans. Nonferrous Met. Soc. China (Engl. Ed.) 30 (2020) 3226–3239, https://doi.org/10.1016/S1003-6326(20)65456-5.
[45] H. Sugo, E. Kisi, D. Cuskelly, Miscibility gap alloys with inverse microstructures and high thermal conductivity for high energy density thermal storage applications, Appl. Therm. Eng. 51 (2013) 1345–1350, https://doi.org/10.1016/J.APPLTHERMALENG.2012.11.029.

[46] C. Confalonieri, E. Gariboldi, Al-Sn miscibility gap alloy produced by power bed laser melting for application as phase change material, J. Alloy. Compd. 881 (2021) 160596, https://doi.org/10.1016/j.jallcom.2021.160596.
[47] C. Confalonieri, R. Casati, E. Gariboldi, Effect of process parameters on laser powder bed fusion of Al-Sn miscibility gap alloy, Quantum Beam Sci. 6 (2022), https://doi.org/10.3390/qubs6020017.
[48] P. Bassani, M. Molteni, E. Gariboldi, Microstructural features and thermal response of granulated Al and A356 alloy with relevant Sn additions, Mater. Des. 229 (2023) 111879, https://doi.org/10.1016/j.matdes.2023.111879.
[49] C. Confalonieri, E. Boller, Y. Cheng, E. Gariboldi, Synchrotron radiation micro-CT with phase contrast for high-temperature in-situ microstructural characterization of Al[sbnd]Sn composite phase change materials, Mater. Charact. 193 (2022) 112302, https://doi.org/10.1016/j.matchar.2022.112302.
[50] H. Pan, Y. Li, H. Zhang, D. Sun, X. Hu, J. Yang, F. Xu, In situ investigation of the healing process in dual-microcapsule self-healing materials by the synchrotron radiation computed tomography, Compos. Part A Appl. Sci. Manuf. 158 (2022) 106955, https://doi.org/10.1016/j.compositesa.2022.106955.
[51] S. Zhang, N. Van Dijk, S. Van Der Zwaag, A review of self - healing metals: fundamentals, design principles and performance, Acta Metall. Sin. (Engl. Lett.) 33 (2020) 1167–1179, https://doi.org/10.1007/s40195-020-01102-3.
[52] C.S.O, P.S. Nnamchi, Exploits, Advances and Challenges in Characterizing Self-Healing Materials, Intech. i, 2016, p. 13.
[53] V. Kilicli, X. Yan, N. Salowitz, P.K. Rohatgi, Recent advancements in self-healing metallic materials and self-healing metal matrix composites, JOM 70 (2018) 846–854, https://doi.org/10.1007/s11837-018-2835-y.
[54] B.B. Straumal, W. Gust, D.A. Molodov, Wetting transition on grain boundaries in Al contacting with a Sn-rich melt, Interface Sci. 3 (1995) 127–132, https://doi.org/10.1007/BF00207014.
[55] Q. Lin, W. Zhong, F. Li, W. Yu, Reactive wetting of tin/steel and tin/aluminum at 350–450 °C, J. Alloy. Compd. 716 (2017) 73–80, https://doi.org/10.1016/j.jallcom.2017.05.036.
[56] A. Rawson, E. Kisi, H. Sugo, T. Fiedler, Effective conductivity of Cu-Fe and Sn-Al miscibility gap alloys, Int. J. Heat Mass Transf. 77 (2014) 395–405, https://doi.org/10.1016/j.ijheatmasstransfer.2014.05.024.
[57] A.J. Rawson, E. Kisi, C. Wensrich, Microstructural efficiency: structured morphologies, Int. J. Heat Mass Transf. 81 (2015) 820–828, https://doi.org/10.1016/j.ijheatmasstransfer.2014.11.012.
[58] E. Gariboldi, M. Perrin, Metallic composites as form-stable phase-change alloys, Mater. Sci. Forum 941 (2018) 1966–1971, https://doi.org/10.4028/www.scientific.net/MSF.941.1966 (MSF).
[59] C. Confalonieri, P. Bassani, E. Gariboldi, Microstructural and thermal response evolution of metallic form-stable phase change materials produced from ball-milled powders, J. Therm. Anal. Calorim. 142 (2020) 85–96, https://doi.org/10.1007/s10973-020-09785-7.
[60] C. Confalonieri, M. Perrin, E. Gariboldi, Combined powder metallurgy routes to improve thermal and mechanical response of Al−Sn composite phase change materials, Trans. Nonferrous Met. Soc. China 30 (2020) 3226–3239, https://doi.org/10.1016/S1003-6326(20)65456-5.
[61] T. Ferreira, W. Rasband, ImageJ User Guide User Guide ImageJ, Image J User Guid. 1.46r, 2012, 10.1038/nmeth.2019.
[62] ThermoCalc ThermoCalc, T.C.S.Al-based Alloy Database (TCAL8), 2021, pp. 1–61.
[63] A. Philipp, J.F. Eichinger, R.C. Aydin, A. Georgiadis, C.J. Cyron, M. Retsch, The accuracy of laser flash analysis explored by finite element method and numerical fitting, Heat Mass Transf. Stoff. 56 (2020) 811–823, https://doi.org/10.1007/s00231-019-02742-7.
[64] G.B. Schaffer, B.J. Hall, The influence of the atmosphere on the sintering of aluminum, Metall. Mater. Trans. A Phys. Metall. Mater. Sci. 33 (2002) 3279–3284, https://doi.org/10.1007/s11661-002-0314-z.
[65] S.R. White, N.R. Sottos, P.H. Geubelle, J.S. Moore, M.R. Kessler, S.R. Sriram, E. N. Brown, S. Viswanathan, Autonomic healing of polymer composites, Nature 409 (2001) 794–797, https://doi.org/10.1038/35057232.
[66] N.A. Dolgopolov, A.L. Petelin, S.V. Rakov, A.V. Simanov, Penetration of liquid tin along grain boundaries and triple grain-boundary junctions of aluminum, Russ. J. Non-Ferr. Met. 48 (2007) 126–130, https://doi.org/10.3103/S1067821207020101.
[67] O.J. Van Der Schijff, N. Budiansky, R.M. Latanision, Liquid-metal- and solid-metal-induced embrittlement, Fail. Anal. Prev. 11 (2021) 573–580, https://doi.org/10.31399/asm.hb.v11.a0006786.
[68] D.G. Kolman, A review of recent advances in the understanding of liquid metal embrittlement, Corrosion 75 (2019) 42–57, https://doi.org/10.5006/2904.
[69] J. Luo, A short review of high-temperature wetting and complexion transitions with a critical assessment of their influence on liquid metal embrittlement and corrosion, Corrosion 72 (2016) 897–910, https://doi.org/10.5006/1925.
[70] V.Alcántara Alza, Spheroidizing in steels: processes, mechanisms, kinetic and microstructure-a review, IOSR J. Mech. Civ. Eng. (IOSR-JMCE) 18 (2021) 63–81, https://doi.org/10.9790/1684-1803036381.
[71] Y.L. Tian, R.W. Kraft, Mechanisms of pearlite spheroidization, Metall. Trans. A. 18 (1987) 1403–1414, https://doi.org/10.1007/BF02646654.
[72] L. Tian, A. Russell, Phase field study of interfacial diffusion-driven spheroidization in a composite comprised of two mutually insoluble phases, J. Chem. Phys. 140 (2014), https://doi.org/10.1063/1.4869296.
[73] C. Confalonieri, E. Boller, Y. Cheng, E. Gariboldi, Synchrotron radiation micro-CT with phase contrast for high-temperature in-situ microstructural characterization of Al[sbnd]Sn composite phase change materials, Mater. Charact. 193 (2022), https://doi.org/10.1016/j.matchar.2022.112302.
[74] S. Sharafat, N. Ghoniem, Summary of Thermo-Physical Properties of Sn, Comparison of Properties of Sn, Sn-Li, Li, and Pb-Li, (n.d.), pp. 1–51.
[75] V.T. Deshpande, D.B. Sirdeshmukh, Thermal expansion of tetragonal tin, Acta Crystallogr 14 (1961) 355–356, https://doi.org/10.1107/s0365110×61001212.
[76] J. FRANCL, W.D. KINGERY, Thermal conductivity: IX, experimental investigation of effect of porosity on thermal conductivity, J. Am. Ceram. Soc. 37 (1954) 99–107, https://doi.org/10.1111/j.1551-2916.1954.tb20108.x.
[77] D.S. Smith, A. Alzina, J. Bourret, B. Nait-Ali, F. Pennec, N. Tessier-Doyen, K. Otsu, H. Matsubara, P. Elser, U.T. Gonzenbach, Thermal conductivity of porous materials, J. Mater. Res. 28 (2013) 2260–2272, https://doi.org/10.1557/jmr.2013.179.
[78] F.C. Nix, D. MacNair, The thermal expansion of pure metals: copper, gold, aluminum, nickel and iron, Phys. Rev. 60 (1941) 597–605.
[79] M.C. Brennan, J.S. Keist, T.A. Palmer, Defects in metal additive manufacturing processes, J. Mater. Eng. Perform. 30 (2021) 4808–4818, https://doi.org/10.1007/s11665-021-05919-6.
[80] E.E. Glickman, On the role of stress, strain and diffusion in dissolution – condensation mechanism of liquid metal embrittlement, Defect Diffus. Forum 264 (2007) 141–149, https://doi.org/10.4028/www.scientific.net/ddf.264.141.
[81] M. Kitamura, K. Hasezaki, Effect of mechanical alloying on thermal conductivity of Bi2Te3-Sb2Te3, Mater. Trans. 57 (2016) 2153–2157, https://doi.org/10.2320/matertrans.M2016169.